



Chitosan-triggered immunity to *Fusarium* in chickpea is associated with changes in the plant extracellular matrix architecture, stomatal closure and remodeling of the plant metabolome and proteome

Kanika Narula^{1,†}, Eman Elagamey^{1,2,†}, Magdi A. E. Abdellatef^{1,2}, Arunima Sinha¹, Sudip Ghosh¹, Niranjan Chakraborty¹ 
and Subhra Chakraborty^{1,*} 

¹National Institute of Plant Genome Research, Aruna Asaf Ali Marg, New Delhi 110067, India, and

²Plant Pathology Research Institute, Agricultural Research Center (ARC), 9 Gamaa St, Giza 12619, Egypt

Received 18 September 2018; revised 29 October 2019; accepted 5 November 2019; published online 14 March 2020.

*For correspondence (e-mail subhrac@hotmail.com).

[†]These authors contributed equally to this study.

SUMMARY

Pathogen-/microbe-associated molecular patterns (PAMPs/MAMPs) initiate complex defense responses by reorganizing the biomolecular dynamics of the host cellular machinery. The extracellular matrix (ECM) acts as a physical scaffold that prevents recognition and entry of phytopathogens, while guard cells perceive and integrate signals metabolically. Although chitosan is a known MAMP implicated in plant defense, the precise mechanism of chitosan-triggered immunity (CTI) remains unknown. Here, we show how chitosan imparts immunity against fungal disease. Morpho-histological examination revealed stomatal closure accompanied by reductions in stomatal conductance and transpiration rate as early responses in chitosan-treated seedlings upon vascular fusariosis. Electron microscopy and Raman spectroscopy showed ECM fortification leading to oligosaccharide signaling, as documented by increased galactose, pectin and associated secondary metabolites. Multiomics approach using quantitative ECM proteomics and metabolomics identified 325 chitosan-triggered immune-responsive proteins (CTIRPs), notably novel ECM structural proteins, LYM2 and receptor-like kinases, and 65 chitosan-triggered immune-responsive metabolites (CTIRMs), including sugars, sugar alcohols, fatty alcohols, organic and amino acids. Identified proteins and metabolites are linked to reactive oxygen species (ROS) production, stomatal movement, root nodule development and root architecture coupled with oligosaccharide signaling that leads to *Fusarium* resistance. The cumulative data demonstrate that ROS, NO and eATP govern CTI, in addition to induction of PR proteins, CAZymes and PAL activities, besides accumulation of phenolic compounds downstream of CTI. The immune-related correlation network identified functional hubs in the CTI pathway. Altogether, these shifts led to the discovery of chitosan-responsive networks that cause significant ECM and guard cell remodeling, and translate ECM cues into cell fate decisions during fusariosis.

Keywords: plant-fungal interaction, extracellular matrix, chitosan-triggered immunity, vascular wilt, chickpea, quantitative proteomics, metabolomics.

INTRODUCTION

The functional association between biomolecules governs the immune response in plants. Regulatory processes linked to chitosan/chitin, pathogen-/microbe-associated molecular patterns (PAMPs/MAMPs) and effector-triggered immunity (ETI), chitosan-triggered immunity (CTI), PAMP-triggered immunity (PTI), MAMP-triggered immunity (MTI) facilitate cellular reprogramming that leads to resistance against pathogen attack.

Chitin oligosaccharides (N-acetyl chitoooligosaccharides), the deacetylated form of chitin, act as archetypal general elicitors and typical fungal MAMPs that induce defense responses in a broad host range, including plants, insects, mice and humans, suggesting the shared occurrence of chitin-mediated defense machinery in higher eukaryotes (Furukawa *et al.*, 1999; Shibuya and Minami, 2001; Reese *et al.*, 2007). Structurally similar to cellulose, chitosan is a basic polycationic, water-insoluble

biopolymer composed of D-glucosamine and N-acetyl D-glucosamine (pKa from 6.2 to 7.0), which exhibits antifungal properties and is found only in fungi possessing deacetylase enzymes (Sankaramakrishnan and Sanghi, 2006). Fatty acids, sulfate, acetyl groups or sugars can modify chitin oligosaccharides and generate 'Nod factors' involved in plant-specific root nodulation during symbiotic interactions with rhizobacteria (Truchet *et al.*, 1991). Previous reports in CTI have focused on the detailed identification and characterization of the chitin high-affinity binding protein viz., Chitin Elicitor Receptor Kinase 1 (CERK1) and CEBiP with lysin motif (LysM) in Arabidopsis, rice, wheat, barley, soybean and carrot (Shibuya *et al.*, 1996; Kaku *et al.*, 1997; Day *et al.*, 2001; Shibuya and Minami, 2001; Tanaka *et al.*, 2010a,b; Fliegmann *et al.*, 2011; Gust *et al.*, 2012; Zeng *et al.*, 2012; Lee *et al.*, 2014; Yin *et al.*, 2016). Chitin-induced signal and immunity nodes, including Rac1, PBL27, LIK1 and RLCK176, have also been characterized and shown to be regulated by phosphorylation events through CERK1 activating small GTPase Rac1, which subsequently governs the MAPK pathway and downstream transcription factors (Akamatsu *et al.*, 2013; Ao *et al.*, 2014; Shinya *et al.*, 2014; Nagano *et al.*, 2016; Yin *et al.*, 2016). In contrast, only a few reports have shown temporal and concentration-dependent effects of chitosan in tobacco and rapeseed development (Guo *et al.*, 2012; Yin *et al.*, 2013, 2016), and induction of pathogen-related (PR) proteins, proteinase inhibitors and phytoalexin in soybean, parsley and pea (Walker-Simmons and Ryan, 1984; Koehle *et al.*, 1985). Amorabé *et al.* (2008) showed that chitosan stimulates a rapid and transient pH increase and depolarization of *Mimosa pudica* motor cell membranes by H⁺-ATPase in a dose-dependent manner, altering carbohydrate and amino acid uptake. Chitosan has been implicated in the defense response in the plant extracellular matrix (ECM) during bacterial infection, including the induction of callose formation, chitinase and glucanase activation, generation of reactive oxygen species (ROS) and lignin synthesis (Roby *et al.*, 1987; Kaku *et al.*, 1997; Okada *et al.*, 2002). These findings indeed suggest that chitosan perception and the immune response may be tightly regulated by post-transcriptional and post-translational mechanisms. However, despite evidence linking chitosan to CTI, the precise cellular mechanism and functional implications underlying its contribution to CTI remain fragmentary to date.

Phytopathogens penetrate the cell either by digesting the cell wall or through wound and natural openings including stomata. Upon pathogen recognition and invasion, plants activate multilayered defense mechanisms, which are not limited to cell wall fortification, ROS release and phytoalexin synthesis (Sankaramakrishnan

and Sanghi, 2006). Plant immunity is known to be governed by five major steps: signal-receptor recognition; signal relay and magnification; activation of defense genes; protein turnover; and reprogramming of defense-related primary and secondary metabolites (Yin *et al.*, 2010). The ECM, the outermost cellular organelle, acts not only as a physical scaffold for the cell, but a dynamic structure that provides the first line of defense in response to disease.

The *Fusarium oxysporum* species complex (FOSC), a soil-borne hemibiotrophic ascomycete fungus, ranking fifth among phytopathogens in economic importance, limits growth and productivity of ~100 plant species. Notably, chitosan has been shown to form physical barriers around penetration sites and inhibits the hyphal growth of many pathogenic fungi, including *F. oxysporum* (Benhamou *et al.*, 1998). In date palm, chitosan treatment leads to enhanced peroxidase and polyphenoloxidase activities with concomitant increases in phenolic compounds in response to FOSC, providing resistance to vascular fusariosis (El Hassni *et al.*, 2004). It has also been implicated as an elicitor of phytoalexin synthesis and an inhibitor of fungal growth in pea–*Fusarium solani* interactions (Hadwiger and Beckman, 1980; Fristensky *et al.*, 1985). Our recent study suggested that CTI and extracellular eATP signaling in the ECM are major players during *F. oxysporum*-induced resistance to vascular wilt in a resistant chickpea cultivar (Elagamey *et al.*, 2017a). Furthermore, we have delineated the vascular wilt-responsive immunome and disease in chickpea using correlation networks into major functional hubs. In the immunome of the resistant cultivar, in addition to PTI and ETI hubs, the CTI module identified chitin-related gene signatures (Ashraf *et al.*, 2018).

Here, we attempted to elucidate the mechanism of chitosan-induced immunity in an otherwise vascular wilt-susceptible chickpea genotype in response to *Fusarium* attack. By comparing physico-chemical and proteo-metabolomic changes in fungal-challenged untreated and chitosan-treated wilt-susceptible and -resistant genotypes, we identified a set of chitosan-responsive proteins and metabolites that might act as key regulatory components imparting immunity against vascular wilt. We further demonstrated that chitosan pre-treatment modulated stomatal functions and the carbohydrate pool in the ECM of the wilt-susceptible genotype. Consistent with the mRNA levels, we observed the induction of defense-responsive proteins, as well as primary and secondary metabolites. ROS, nitric oxide (NO), eATP and ion transport clearly governed chitosan-induced root nodule and secondary root formation in patho-stressed seedlings. However, in the wilt-resistant genotype, molecular responses to chitosan pre-treatment were almost the

same as in untreated seedlings in response to fungal attack. These results revealed that oligosaccharide signaling, enhanced NO and eATP are essential for chitosan-induced wilt resistance.

RESULTS

Chitosan affects root architecture and inhibits fungal growth

To understand whether chitosan displays antifungal activity against *F. oxysporum*, the fungal inoculum was grown on potato dextrose agar (PDA) containing different concentrations of chitosan. Interestingly, chitosan at increasing concentrations from 0.1 to 0.6 mg L⁻¹ reduced fungal growth *in vitro*. The maximum reduction (70%) was observed at 0.6 mg L⁻¹ (Figure 1a). Previous studies have also supported its antifungal and antibacterial activity *in vitro* (Alburquenque *et al.*, 2010; Rahman *et al.*, 2015; Goya *et al.*, 2016). Our group and others have identified cv. WR-315 and cv. JG-62 as the most wilt-resistant and wilt-susceptible chickpea genotypes, respectively (Jiménez-Díaz *et al.*, 1989; Thaware *et al.*, 2016; Ashraf *et al.*, 2018). Next, to assess the effect of chitosan on *in planta* inhibition of *F. oxysporum* pathogenesis in the susceptible genotype JG-62, four datasets were examined based on chitosan pre-treatment (C+) or not (C-) of wilt-resistant and -susceptible genotypes prior to *Fusarium* challenge (F+). The results revealed highly reduced wilting and disease severity (56–85% at 120–480 hpi) in the C+F+ wilt-susceptible genotype similarly to the C-F+ wilt-resistant genotype when compared with the C-F+ wilt-susceptible genotype. However, C-F+ and C+F+ displayed a similar level of resistance in the wilt-resistant genotype (Figure 1b,c). Quantitative examination of fungal progression revealed that C-F+ and C+F+ WR-315, C+F+ JG-62 showed a 50% decrease in fungal biomass across the time points when compared with C-F+ JG-62 (Figure 1d). Furthermore, lipid peroxidation is a major biochemical change during fungal attack leading to pathogen colonization and invasion. Importantly, similar to C-F+ and C+F+ WR-315, C+F+ JG-62 showed a significant decrease in electrolyte leakage during *Fusarium* attack preventing fungal invasion (Figure 1e). Concomitantly, chitosan triggered root nodule formation and lateral or secondary root formation during fusariosis (Figure S1a). Following these observations, we determined the proline level and relative water content (RWC) of C-F+ and C+F+ WR-315 and JG-62. Both C-F+ and C+F+ WR-315 and C+F+ JG-62 were able to maintain a higher concentration of proline and similarly higher level of RWC (~66% recovery in RWC), suggesting an increased water uptake ability in C+F+ JG-62 as fungal colonization was considerably reduced in the xylem vessel (Figure S1b,c).

Chitosan modulates the ECM ultrastructure and carbohydrate composition during *Fusarium* attack

Chitosan had been linked to callose deposition in the cell wall during pathogen attack (Iriti and Faoro, 2009). To examine whether chitosan dictates ECM reinforcement, the collar region of C-F+ and C+F+ WR-315 and JG-62 seedlings was examined using scanning electron microscopy. In response to patho-stress, C-F+ JG-62 seedlings showed intensive wall deformation during fungal invasion up to 480 hpi. However, C-F+ and C+F+ WR-315 and C+F+ JG-62 seedlings exhibited comparable time-dependent wall thickening, indicating that chitosan prevented wall deformation during *Fusarium* attack. The observed changes in ECM ultrastructure upon chitosan treatment might play an important role in imparting mechanical strength and resistance to the invading fungal mycelia (Figure 2a). To study changes in the molecular composition of the ECM, we performed confocal Raman spectroscopy in both C-F+ and C+F+ WR-315 and JG-62 seedlings in a temporal manner. By integration of wavenumbers with strong Raman bands, two-dimensional chemical spectra were determined, which identified lignin, cellulose and pectin as dominant species (Figure 2b). The spectrum at 900 cm⁻¹ (903–997 cm⁻¹) and 1600 cm⁻¹ (1550–1640 cm⁻¹) bands showed that the lignin distribution was dominated by the aromatic C5C vibration (Figure 2c). The cellulose orientation-sensitive band was obtained by integration of a narrow wavenumber area at 1026–1180 cm⁻¹, whereas the presence of the Raman band at 515 and 854 cm⁻¹ indicated the presence of pectin in patho-stressed seedlings (Figure 2c). Quantitative analysis of these carbohydrate molecules revealed a marginal change in the dry matter of cellulose and lignin between C-F+ and C+F+ JG-62 and WR-315 seedlings (Figure 2d). Interestingly, the percent dry matter of pectin showed a significant increase (15%) up to 480 hpi in C+F+ JG-62 in comparison to C-F+ JG-62. However, chitosan treatment showed no significant change in the pectin content of WR-315 seedlings during *Fusarium* attack. These data suggest a role of pectin as a crucial ECM component in first-level defense and chitin-triggered immunity.

Metabolic status of chitosan-treated patho-stressed seedlings correlates with morpho-histology and ECM dynamics

To test whether, in addition to carbohydrates, other metabolic compounds were also affected in C+F+ JG-62 and WR-315 compared with their C-F+ seedlings, we performed gas chromatography-mass spectrometry (GC-MS). Metabolite profiling identified kinetically controlled distinct and reproducible differences (Figure 2e). In total, 68 and 70 metabolites were detected in C-F+ and C+F+ JG-62, respectively, while 70 and 72 metabolites were identified in the C-F+ and C+F+ wilt-resistant genotype, respectively. Of

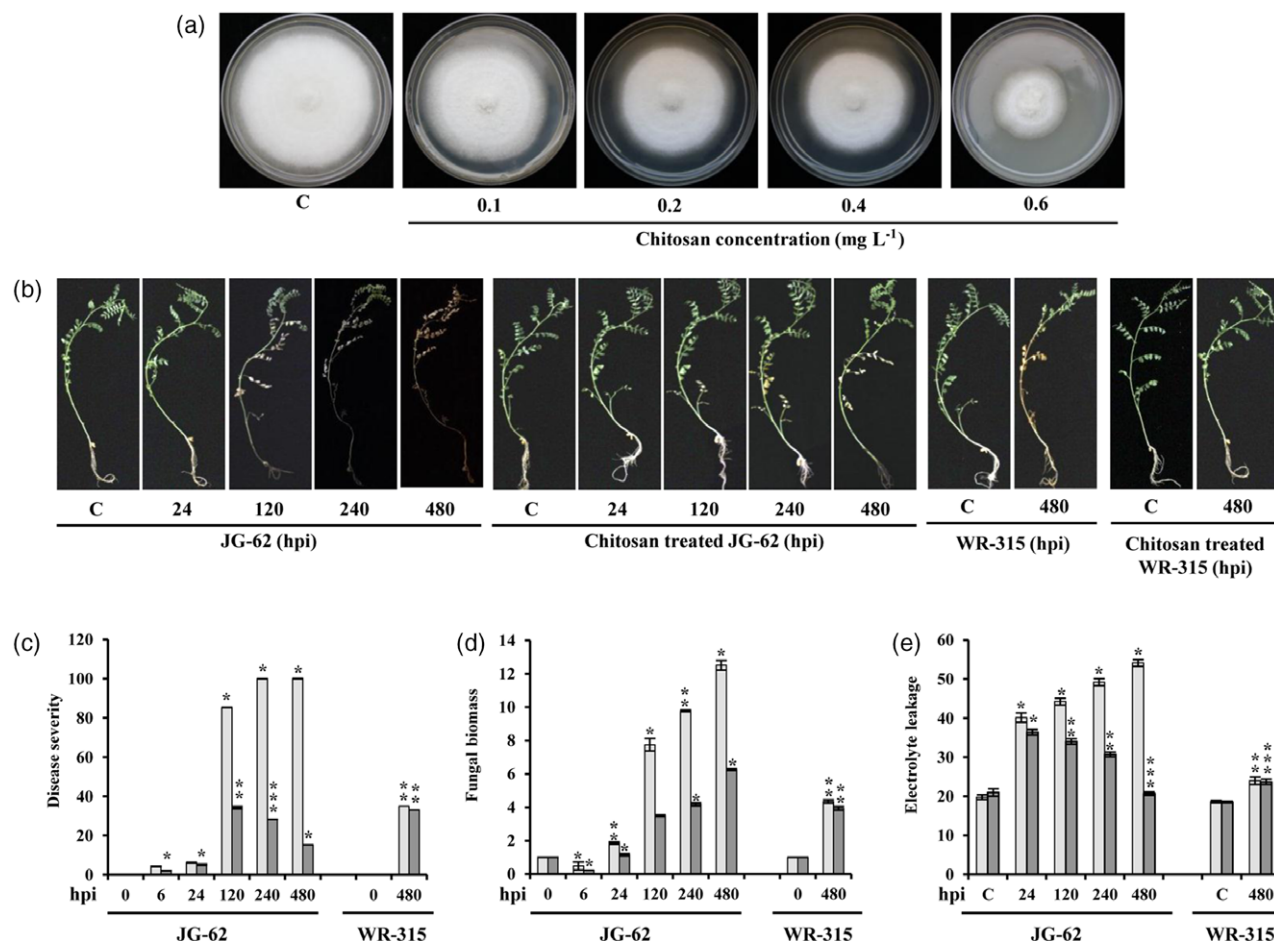


Figure 1. Effect of chitosan on chickpea seedlings challenged with *Fusarium oxysporum*.

(a) Fungal growth inhibition at different concentration of chitosan on potato dextrose agar (PDA).

(b) Photographs showing C–F+ and C+F+ JG-62 and WR-315 chickpea seedlings.

(c) Measurement of disease severity.

(d) Relative quantification of fungal biomass by real-time polymerase chain reaction (PCR) on DNA extracted from *F. oxysporum*-infected seedlings of chitosan-treated and untreated JG-62 at 6, 24, 120, 240 and 480 hpi, and without and with chitosan-treated WR-315 seedlings at 480 hpi. Amplification values for FoGDP were normalized to the abundance of chickpea 18S sequence.

(e) Estimation of electrolyte leakage. Four independent experiments were performed with three biological replicates each consisting of five plants. Vertical bars represent means of 12 biological replicates. Error bars indicate SD of mean ($n = 12$). Black bar denotes that seedlings were treated with chitosan, and gray bar represents seedlings without chitosan treatment. Expression changes were analyzed by ANOVA and Tukey *post hoc* test ($P < 0.05$). *Indicates statistical significance of relative amount of fungal DNA.

the 61 common metabolites, between C–F+ and C+F+ JG-62 across time points, 45 (74%) and 50 (81%) were upregulated, whereas 16 (26%) and 11 (18%) were downregulated,

respectively. The C–F+ and C+F+ wilt-resistant genotype had 58 common metabolites, with 41 and 43 metabolites showing upregulation and 17 and 15 displaying

Figure 2. Extracellular matrix (ECM) ultrastructure and carbohydrate composition changes in chitosan-treated and untreated JG-62 seedlings, and without and with chitosan-treated WR-315 during *Fusarium* attack.

(a) Scanning electron micrograph (SEM) illustrating ECM ultrastructural changes. Scale bar: 20 μm .

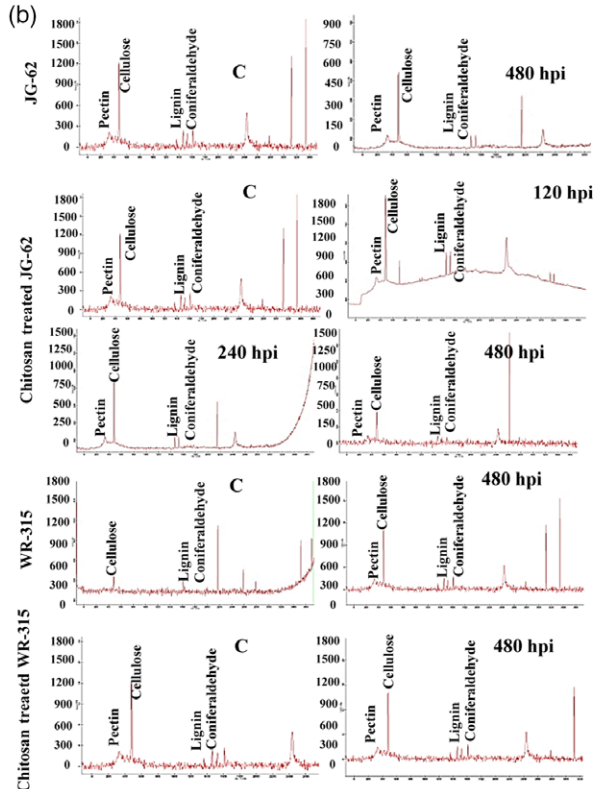
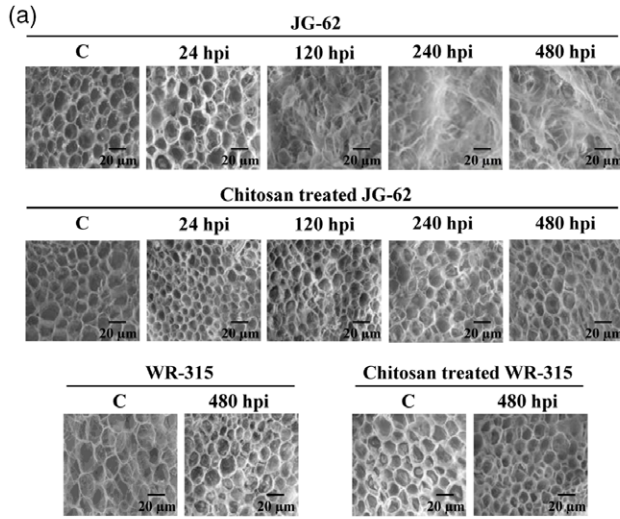
(b) Raman spectra of chickpea seedlings in response to *Fusarium*.

(c) Description of wave number and detected carbohydrate component.

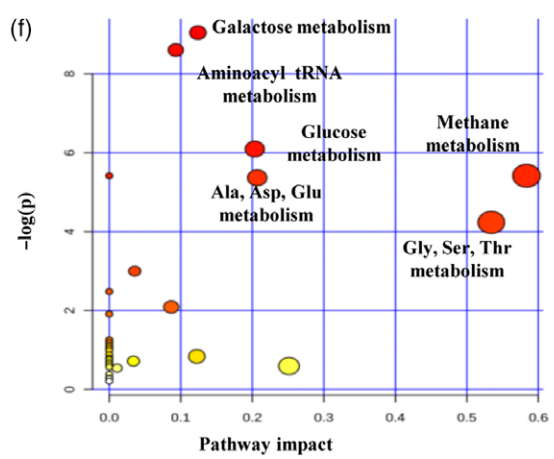
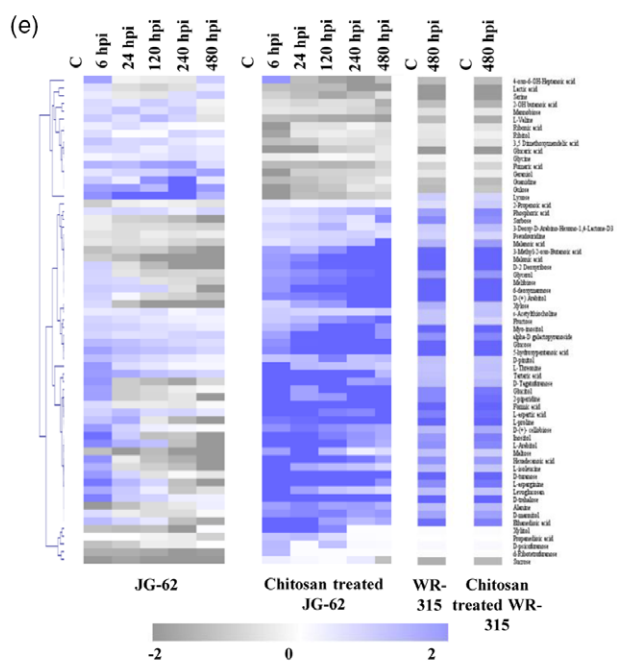
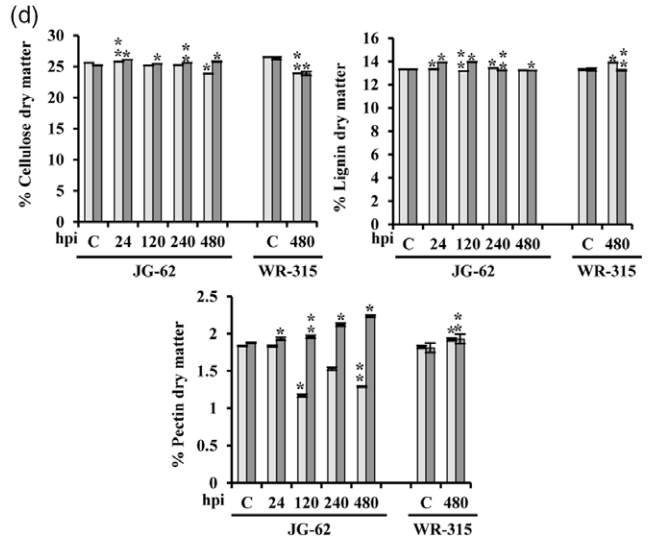
(d) Estimation of % cellulose, % pectin and % lignin dry matter. Four independent experiments were performed with three biological replicates each consisting of five plants. Vertical bars represent means of 12 biological replicates. Error bars indicate SD of mean ($n = 12$).

(e) Metabolite analysis of chitosan-treated chickpea seedlings and its comparison to without chitosan-treated seedlings during *Fusarium* attack and hierarchical clustering analysis of immune-responsive metabolites (IRMs), chitosan-triggered immune-responsive metabolites (CTIRMs) and disease-responsive metabolites (DRMs).

(f) Pathway impact analysis. Changes were analyzed by ANOVA and Tukey *post hoc* test ($P < 0.05$), and vertical bars indicate SD. Black bar denotes that seedlings were treated with chitosan, and gray bar represents seedlings without chitosan treatment. *Indicates statistical significance at $P < 0.05$.



| Wave number (cm ⁻¹) | Component |
|---------------------------------|-------------------------|
| 515–523 | Pectin |
| 854 | Pectin |
| 903–905 | Lignin |
| 997 | Lignin |
| 1026–1129 | Cellulose |
| 1274 | Guaicyl ring, lignin |
| 1333–1376 | HCC bending, cellulose |
| 1508 | Aryl ring, lignin |
| 1601 | Aryl ring, lignin |
| 1620–1660 | Coniferaldehyde, lignin |
| 2810–2897 | Cellulose |
| 2945 | Gluc Mann, lignin |



downregulation in the respective genotypes. Consistent with the morpho-histological indices, a significant difference in the metabolite profile was observed with a high accumulation of sugar, sugar alcohol and fatty alcohol in C+F+ JG-62, similar to C-F+ and C+F+ WR-315 seedlings. Interestingly, the constituents of wall carbohydrates, including glucose (threefold), fructose (2.5-fold), D-psicofuranose (0.95-fold), sorbose, D-ribo-tetrofuranose (0.91-fold), galactose (3.6-fold), xylose (3.12-fold) and D-(+)-cellobiose (threefold), were significantly increased in C+F+ JG-62 seedlings. In addition, comparable to C-F+ and C+F+ WR-315, the osmoprotectant D-(+)-trehalose, glycerol, proline and xylitol were also increased five–10-fold, probably to maintain the RWC of C+F+ JG-62 seedlings. The twofold increased level of the antioxidant D-(–)-tagatofuranose suggested that chitosan might govern redox homeostasis. Immunity-priming metabolites, including melibiose, D-mannitol, arabitol, geraniol and 4-oxo-6-OH-heptanoic acid, exhibited elevated levels in C-F+ and C+F+ wilt-resistant and C+F+ wilt-susceptible genotypes. Nonetheless, the C-F+ wilt-susceptible genotype showed lower levels of immunity-priming metabolites during fungal attack. It is well known that interplay between myo-inositol metabolism, redox status and programmed cell death (PCD) dictates basal immunity in plants (Meng *et al.*, 2009). Fatty acids are known to be linked to the carbohydrate moiety in the plant matrix (Voxeur and Fry, 2014). We observed a three–sevenfold increase in hexadecanoic acid, which might promote wall strength. Metabolites related to organic acid biosynthesis, which have roles in plant basal defense, were also detected at high levels, including 2-OH butanoic acid. Moreover, primary amino acids that are known to modulate plant immunity, such as L-asparagine, L-aspartic acid and L-isoleucine, were found at high levels in chitosan-treated seedlings. Phenylalanine and propane-dioic acid, the precursors for phenylpropanoids and galactose, were also found in high abundance in C+F+ JG-62 and WR-315 seedlings, suggesting roles for lignin and pectin in chitosan-mediated immunity. Indeed, C+F+ JG-62 and WR-315 seedlings showed a marginal increase in lignin; however, pectin was increased 1.5–1.7-fold when compared with C-F+ JG-62 seedlings. Finally, to understand the pathway impact of particular biosynthetic processes, we determined the statistical significance of the metabolites. Interestingly, metabolites related to galactose and glucose biosynthetic processes had significant pathway impact in response to chitosan during *Fusarium* attack (Figure 2f).

The quantitative ECM proteome reveals the molecular basis of chitosan-induced immunity

We recently reported the ECM proteome of the wilt-resistant chickpea cultivar WR-315, which indicated cell wall reprogramming is an important driver of host-specific

immunity during *Fusarium* attack (Elagamey *et al.*, 2017a). To uncover the molecular phenomena underlying vascular wilt resistance due to chitosan treatment and its relation to metabolic dynamics, we developed comparative ECM proteomes of the C-F+ and C+F+ wilt-susceptible and C-F+ wilt-resistant genotypes. Temporal ECM proteomic changes were monitored using iTRAQ coupled with liquid chromatography-tandem mass spectrometry (LC-MS/MS). We identified 287 disease-responsive proteins (DRPs), 325 chitosan-triggered immune-responsive proteins (CTIRPs) and 325 immune-responsive proteins (IRPs) in C-F+ JG-62, C+F+ JG-62 and C-F+ WR-315, respectively, at a false discovery rate (FDR) < 1% and $P < 0.05$ from three biological replicates. Of these proteins, 252 proteins (87%) and 255 proteins (78.4%) were distinct, while 13 and 21.6% were either post-translationally modified forms or multi-gene family members in C-F+ and C+F+ JG-62 seedlings, respectively (Figure 3a; Table S1a–c). A total of 325 IRPs were mapped to 253 distinct proteins in C-F+ WR-315 seedling (Figure 3a; Table S1c). In total, 54 DRPs, 66 CTIRPs and 187 IRPs were induced, 73 DRPs, 11 CTIRPs and 138 IRPs showed repression, and 160 DRPs and 248 CTIRPs exhibited a mixed abundance during *Fusarium* infection (Figure 3b). Interestingly, CTIRPs and IRPs showed similar expression profile trends, whereas opposite protein abundance patterns were observed between DRPs and CTIRPs involved in wall biogenesis, redox homeostasis, signaling and defense. CTIRPs related to miscellaneous function, including Bet1 protein, were repressed, and peroxidase family proteins and purple acid phosphatase were upregulated, pointing towards a role for ROS signaling in chitosan-induced wilt resistance (Figure 3b). To determine the putative functions of unknown proteins, domain analysis was performed using the InterPro, Panther and Pfam database (Table S2a,b). Among the proteins identified, 13, 32 and 62 were increased by more than 2.5-, 2.0- and 1.5-fold, respectively, in the C-F+ wilt-susceptible genotype. In addition, 27, 40 and 90 proteins displayed more than 2.5-, 2.0- and 1.5-fold increases, respectively, in the C+F+ wilt-susceptible genotype. In contrast, the C-F+ wilt-susceptible genotype had 23, 26 and 82 proteins with decreased abundance, whereas the C+F+ wilt-susceptible genotype had 12, 43 and 72 proteins with decreased abundance to less than 0.40-, 0.50- and 0.67-fold, respectively. Chitin-degrading enzymes, namely, acidic endochitinase, endochitinase, endochitinase A2-like and chitinase 2, showed increased expression in the C-F+ wilt-resistant genotype and C+F+ wilt-susceptible genotype, which have previously been shown to be involved in CTI (Itoh *et al.*, 2013). Interestingly, three disease-resistance response proteins (gi|502147529, gi|502147532, gi|502109348), pathogenesis-related protein PR-4A (gi|502117390) and thumatin-like pathogenesis-related protein 4 (gi|502139400) were highly increased by more than threefold in both C-F+

resistant and C+F+ susceptible cultivars. However, chitin-degrading enzymes and disease-resistance protein showed decreased expression in the C–F+ wilt-susceptible genotype, favoring fungal pathogenesis. In the presence of chitin, LysM domain-containing GPI-anchored protein 2-like (LYM2) is known to mediate the reduction of molecular flux through plasmodesmata (Faulkner *et al.*, 2013). Further, CAZy enzymes are strongly related to maintenance of the carbohydrate flux and oligosaccharide signal transduction (Paull *et al.*, 2016). According to the differential ECM proteomic analysis, in our study, LYM2 (gi|502141811) and CAZy enzymes: alpha-galactosidase (gi|502104561), α -L-arabinofuranosidase (gi|502107566), α -L-fucosidase (gi|502082094), α -mannosidase (gi|502106849), β -fructofuranosidase (gi|502156268) and β -glucosidase (gi|502081670) were highly increased by 1.2-, 4.5-, 3.7-, 4.8-, 5.4-, 10.6- and 12.1-fold, respectively, in the C+F+ susceptible and C–F+ resistant genotypes. Increased levels of these proteins might maintain the ECM carbohydrate meshwork during fungal attack, corroborating the results of metabolite profiles and Raman spectroscopy. LYM2 and CAZy enzymes showed an opposite ECM protein expression pattern in the C–F+ wilt-susceptible genotype, indicating extensive wall deformation during fungal attack. Several proteins with known miscellaneous functions were significantly decreased in the C+F+ susceptible and C–F+ resistant cultivars, including staphylococcal nuclease domain-containing protein 1 (gi|502137291; 0.07-fold), ferredoxin-dependent glutamate synthase 1 (gi|502108182; 0.13-fold), fructose-bisphosphate aldolase 1 (gi|502149386; 0.06-fold) and glycine cleavage system H protein (gi|502160535; 0.04-fold). Subtilisin-like protease (gi|502131251) and aspartic protease 2 (gi|502133045) representing components of the ECM homeostasis machinery showed decreased expression by 0.2- and 0.09-fold, respectively. Quinone oxidoreductase (gi|502154752), which is necessary to induce haustorium development (Bandaranayake *et al.*, 2010), was decreased by 0.15-fold in the C+F+ wilt-susceptible and C–F+ wilt-resistant genotypes, while it was increased in the C–F+ wilt-susceptible genotype. Chitosan also altered pectin-modifying ECM remodelers and ROS enzymes at the protein level. We detected a reduction of pectinesterase (gi|54303968, gi|502103214, gi|50217052) and induction of probable pectinesterase/pectinesterase inhibitor 40-like (gi|502112620) and polygalacturonase inhibitor (gi|502141978) during a later phase of fungal attack in the C+F+ wilt-susceptible genotype. Further, the protein profiles of ROS enzymes revealed that different classes of peroxidases (gi|502129543, gi|502077140, gi|502118925), 2-Cys peroxidase (gi|502122295) and L-ascorbate oxidases (gi|502144383, gi|502134017) were induced during a later phase of fungal attack in the C+F+ wilt-susceptible and C–F+ wilt-resistant genotypes. However, ROS machinery components, including amine oxidase (gi|55977746),

lactoylglutathione lyase (gi|502079139) and superoxide dismutase (SOD) [Cu-Zn] (gi|502145557), showed increased expression in the early and middle phase of *Fusarium* attack in C+F+ wilt-susceptible and C–F+ wilt-resistant genotypes. The disease-responsive ECM proteome of the C–F+ wilt-susceptible genotype showed reduced expression of pectin-modifying enzymes and ROS machinery during pathogenesis. These results suggest that chitosan treatment might govern CTI and oligosaccharide signaling associated with ECM proteins and redox homeostasis during fungal pathogenesis.

Defining biological processes and the molecular functionality of core ECM CTIRPs

To estimate significant variability between fungal-challenged susceptible and chitosan pre-treated susceptible genotypes as for the resistant cultivar, 287 DRPs and 325 CTIRPs and IRPs were subjected to principal component analysis (PCA). A Scree plot depicted variation in four principal components between the control and disease/immune state (Figure 3c). PCA biplot analysis of 287 DRPs resulted in the plotting of PC1 (42.15%) against PC2 (18.12%), while 325 CTIRPs and IRPs resulted in the plotting of PC1 (45.52%) against PC2 (20.93%) segregated proteins into three groups. Group I (C1) included 2 DRPs, 5 CTIRPs and 5 IRPs with increased expression related to the disease response and innate defense involving CTI components. Group II (C2) of 1 DRP, 3 CTIRPs and 3 IRPs showed induction, while group III (C3) comprising 1 DRP, 2 CTIRPs and 2 IRPs showed a mixed abundance indicating that CTI was regulated by the coordination of proteins belonging to diverse functional categories. In the biplot of 287 DRPs, the main segregation was observed for proteins involved in wilt disease. To gain further insight into the regulatory and functional roles of DRPs, CTIRPs and IRPs, we sorted them into seven functional categories, among which 12% and 16% DRPs and 8% and 21% CTIRPs and IRPs were designated as unknown and miscellaneous proteins, respectively (Figure 3d). A comparison of the functional annotation categories of DRPs, CTIRPs and IRPs showed that the major functional groups corresponded to oxidoreductase (20%) followed by proteins acting on carbohydrates (12–16%). Other important categories included proteases (10–11%), proteins involved in lipid metabolism (7–13%), signaling (6–7%), innate defense (5–7%) and proteins with interacting domains (2–4%). Furthermore, we used the bioinformatics platforms for Blast2GO term analyses and the Kyoto Encyclopedia of Genes and Genomes (KEGG) database for metabolic pathway analyses. The data revealed diverse biological processes exhibiting distinct molecular functions (Figures 3d and S2). Notably, DRPs, CTIRPs and IRPs associated with ECM functionality, particularly GO terms related to organic substances, primary metabolic process, oxidation–reduction, nitrogen

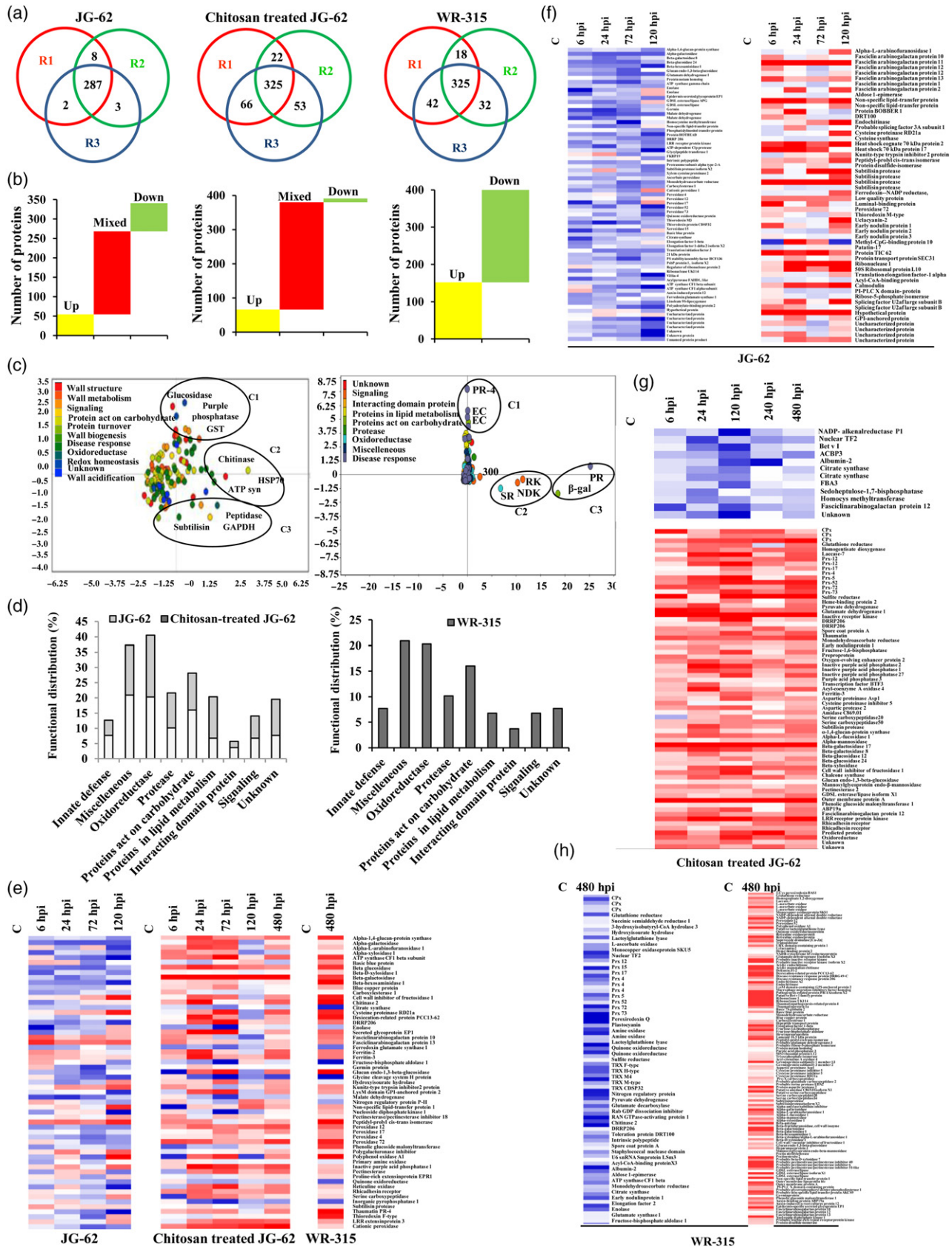


Figure 3. Comparative extracellular matrix (ECM) proteome analysis of chitosan-treated and untreated JG-62 and WR-315 seedlings infected with *Fusarium*. (a) Venn diagram showing overlap of disease-responsive proteins (DRPs), chitosan-triggered immune-responsive proteins (CTIRPs) and immune-responsive proteins (IRPs). (b) Water fall graph depicting regulation of DRPs, CTIRPs and IRPs. (c) Principal component analysis (PCA) biplot of DRPs, CTIRPs and IRPs. X- and Y-axes represent distance from first (F1) and second (F2) principal components, respectively. Different colors represent functional category of ECM proteins. Outlier spots are denoted by circles. (d) Functional classification of DRPs, CTIRPs and IRPs. (e–h) Heat map of the DRPs, CTIRPs and IRPs according to their functional and up/downregulation. Each protein is represented by a single row of colored boxes, and each time point is represented by a single column. Induction or repression ranges from red to saturated shades of blue, respectively.

compound process, macromolecule carbohydrate, protein, small molecule, cellular and cofactor metabolic process, accounted for 61%, 59% and 60% biological function, respectively. Interestingly, the major overrepresented molecular functions of DRPs, CTIRPs and IRPs were hydrolase activity, oxidoreductase activity, ion binding, cation binding, catalytic activity, organic cyclic compound binding and coenzyme binding accounting for 79%, 82% and 83%, respectively.

To differentiate between key molecular effects of chitosan on *Fusarium* attack, we examined the co-expression dynamics of DRPs, CTIRPs and IRPs using a heat map and hierarchical clustering (Figures 3e–h, S3 and S4). The heat map demonstrated an individual heterogeneity of protein expression profiles among different ECM proteomic datasets. Interestingly, DRPs exhibiting reduced expression corresponded to ROS and eATP signaling component candidates. CTIRPs and IRPs showing early increases in abundance were more likely to represent oligosaccharide signaling components candidates than late-expressing proteins, potentially signifying secondary alterations due to perturbed cellular protein homeostasis. DRPs, CTIRPs and IRPs predicted 10 expression clusters, of which $n > 6$ were considered for further analysis (Figures S3 and S4). Clustering of DRPs suggested that Clusters 2 and 7 mainly comprised upregulated proteins belonging to the disease response and proteases. DRPs with reduced expression were grouped in Clusters 1, 3 and 6 associated with wall biogenesis, redox homeostasis and signaling. These results further indicated that the most abundant Clusters 8, 3, 9 and 1 comprised upregulated CTIRPs and IRPs related to oxidoreductases, miscellaneous and signaling categories. Other predominant groups were Clusters 2 and 4 comprising proteins participating in carbohydrate and protein homeostasis, which exhibited mixed expression. Clusters 5 and 6 included CTIRPs and IRPs, which exhibited decreased abundance in the later phase of fungal attack. Cluster 7 mainly involved CTIRPs and IRPs, such as proteases, proteins involved in lipid metabolism and proteins with an interacting domain, followed by the immune response with increased abundance during the later and middle phases of fungal attack. Together these results suggested that chitosan-induced immunity in *Fusarium* wilt was largely governed by different co-expressed proteins

belonging to oligosaccharides, lipids and secondary metabolism during the early, middle and later phases of pathogen challenge.

Characterization of the transcript accumulation of CTIRPs, IRPs and DRPs affected by *Fusarium* attack

Given the large number of statistically significant CTIRPs, IRPs and DRPs in the ECM proteome, we investigated whether small changes in protein expression could be biologically relevant at a specific phase or at multiple steps within the same phase, as conceptualized by biochemical and metabolic analyses. First, we enlisted CTIRPs, IRPs and DRPs that showed > 1.5 -fold changes in expression between C–F+ and C+F+ JG-62, and C–F+ WR-315 at any particular phase of *Fusarium* attack (Table S1). In addition to the fold-change analysis, a *t*-test set at $P < 0.01$ was performed to compare a specific phase of *Fusarium* invasion between the two cultivars. A volcano plot was generated to infer the relationship between the *P*-value from the *t*-test and the fold difference at different phases of fungal attack (Figures 4a and S5). CTIRPs, IRPs and DRPs, selected from the plots, showed significant differences between the C–F+ and C+F+ wilt-susceptible genotype compared with the C–F+ wilt-resistant genotype during different phases of fungal attack. Most of the observed differences occurred during the early and middle phases. CTIRPs, IRPs and DRPs associated with oligosaccharide signaling, ROS signaling and innate defense showed significant differences in different phases of pathogenesis. The maximum difference in the normalized intensity was seven-, six- and 13-fold at different phases of pathogen attack in C–F+ and C+F+ JG-62, and C–F+ WR-315 seedlings, respectively. β -Galactosidase 8-like and endochitinase were expressed at sixfold higher levels at 240 hpi in C+F+ JG-62, while endochitinase showed an 11-fold increase in C–F+ WR-315; the minimum fold difference of 0.06 was observed at 120 and 240 hpi in C+F+ JG-62. DRPs, which were involved in protein turnover and the disease response, such as peptidyl-prolyl cis-trans isomerase, kunitz-type trypsin inhibitor 2 and polyphenol oxidase A1, exhibited 1.5–3.0-fold increases up to 120 hpi in C–F+ JG-62. ROS-associated peroxidase family members were accumulated to a significantly higher level in both patho-stressed cultivars. Intriguingly, the purinergic signal component purple acid

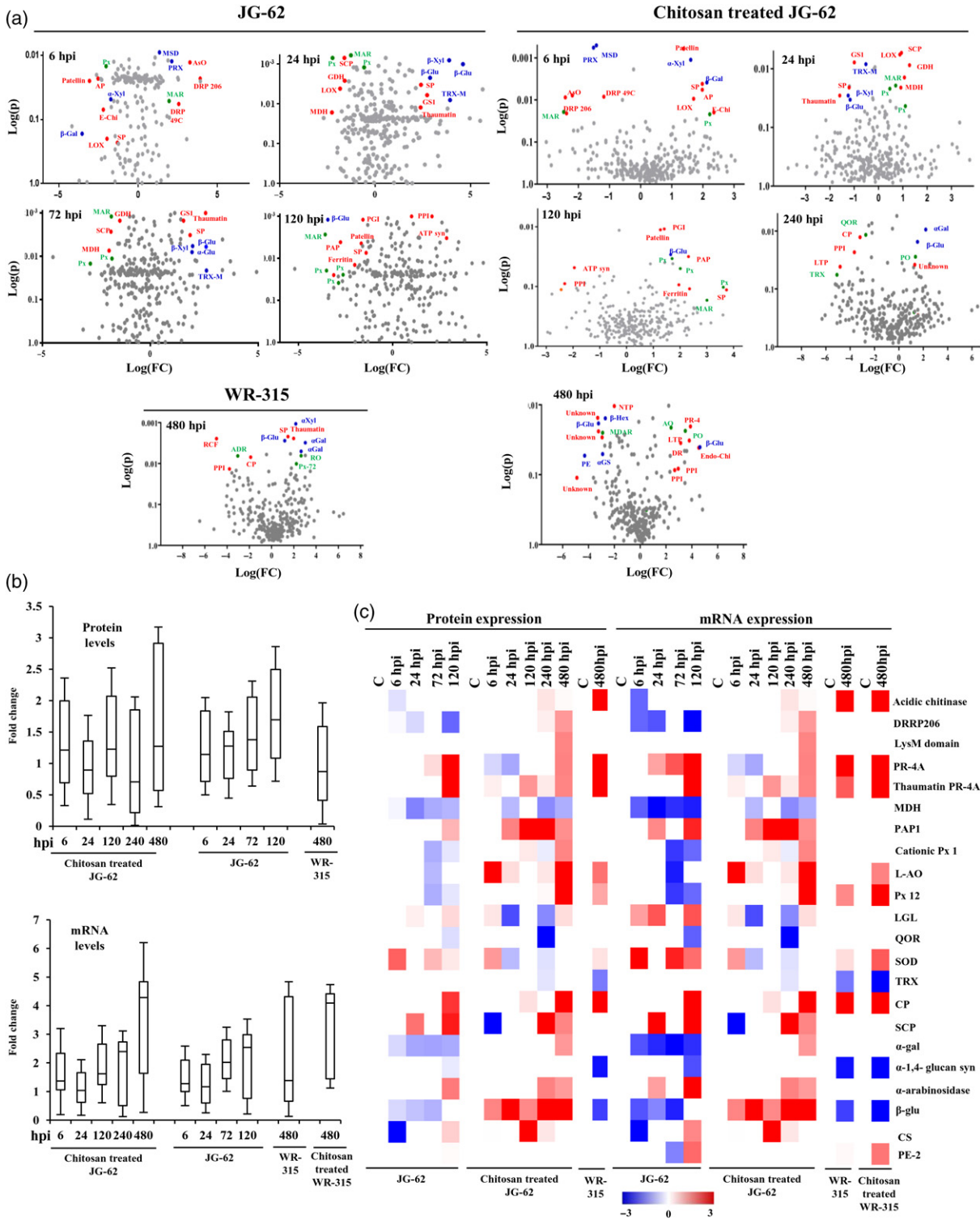


Figure 4. Comparison of protein abundance and mRNA levels.

(a) Relationships between the 1.5-fold difference and statistical significance using *t*-test are presented by volcano plots for each time point, the disease-responsive proteins (DRPs), chitosan-triggered immune-responsive proteins (CTIRPs) and immune-responsive proteins (IRPs) with the greatest significant difference are shown based on function as red (innate defense), green (redox homeostasis) and blue (carbohydrate reorganization).

(b) Box whisker plot showing the range of coverage of DRPs, CTIRPs and IRPs, and respective mRNA within each time point.

(c) Analysis of levels of proteins and mRNA. Relative quantification (RQ) of mRNA levels was performed on candidate DRPs, CTIRPs and IRPs by quantitative reverse transcriptase-polymerase chain reaction (qRT-PCR). Experiments were performed in three replicates. Expression changes were analyzed by ANOVA.

phosphatase, which is known to be involved in eATP biogenesis, exhibited a threefold increase in C+F+ JG-62, confirming that chitosan-induced eATP signaling might lead to wilt resistance.

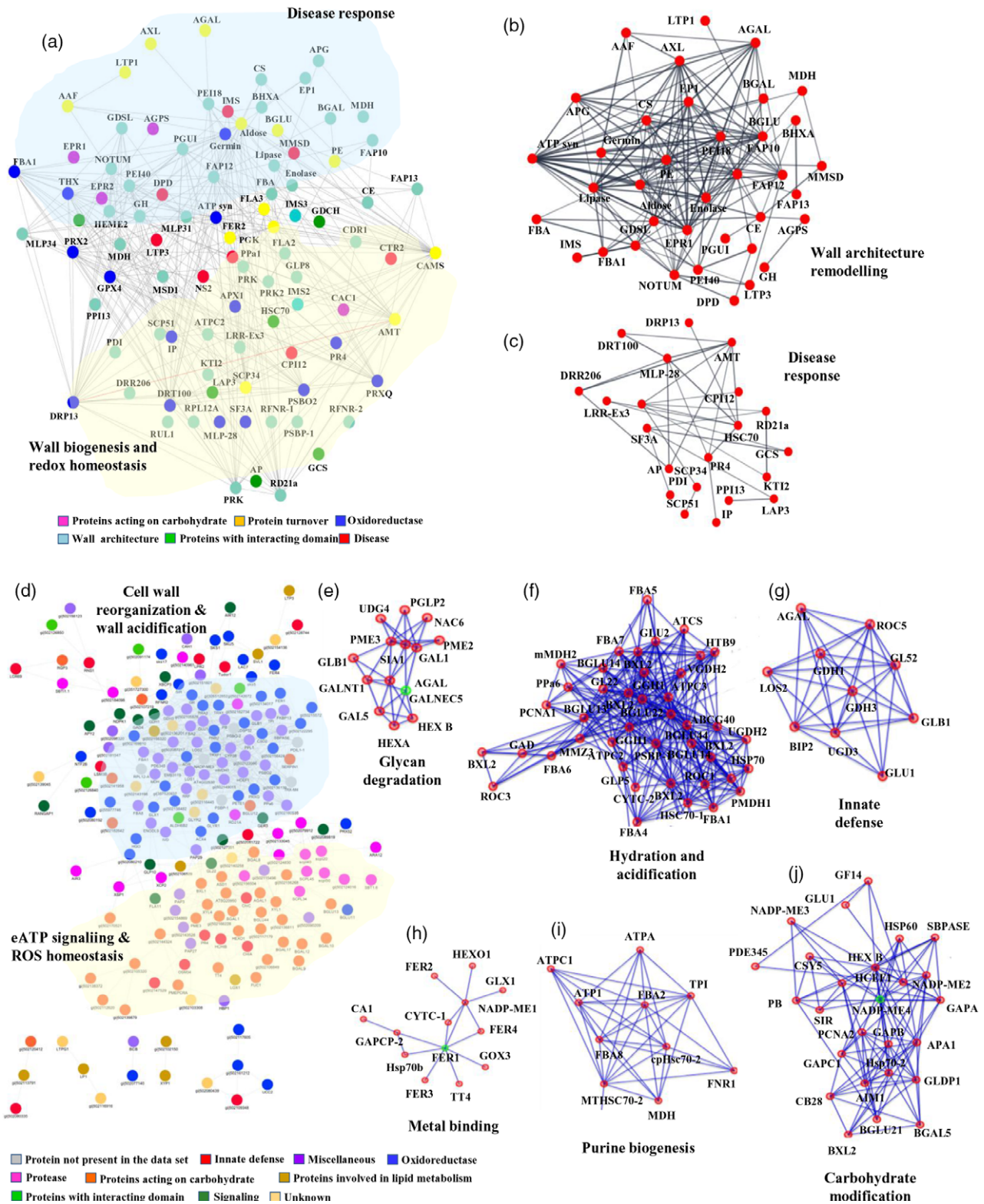
To determine the correlation between protein expression and the corresponding mRNA abundance, 25 significant and common proteins among CTIRPs, IRPs and DRP, based on PCA and volcano plots, either previously reported to be involved in disease/immune response or found to be unique in our study, were selected for quantitative reverse transcriptase-polymerase chain reaction (qRT-PCR) analysis (Figure 4b,c). Expression levels of the oligosaccharide signaling components viz., chalcone synthase, β -glucosidase 12 and acidic mammalian chitinase, and ROS signaling components, including SOD [Cu-Zn], lactoylglutathione lyase, quinone oxidoreductase-like protein and L-ascorbate oxidase, were upregulated in the early stage in C+F+ JG-62 and C-F+ WR-315 seedlings. However, these proteins and corresponding mRNAs were downregulated in C-F+ JG-62. CTIRPs such as α -1,4-glucan-protein synthase, enolase, inactive purple acid phosphatase 1, cationic peroxidase 1-like and thioredoxin-like protein were significantly induced in the middle stage of fungal attack, whereas pectinesterase 2-like, alpha-L-arabinofuranosidase 1, alpha-galactosidase-like isoform X1, serine carboxypeptidase, disease-resistance response protein 206, LYM2, pathogenesis-related protein PR-4A, thaumatin-like PR-4, peroxidase 12, cysteine proteinase RD21a and glutathione reductase (GR) were upregulated during the later phase of fungal attack. Opposite trends in the expression profiles of DRPs and corresponding mRNAs as against CTIRPs and IRPs were also observed. The data were in agreement with the proteome analysis showing an analogous expression profile as the mRNA counterparts. Next, we determined the correlation in ECM protein abundance and compared them with their respective mRNA levels. Box whisker plots showing the coverage of CTIRPs, IRPs and DRPs and respective mRNAs across time points represent the median value falling in the range from 24 to 78% within the box (Figure 4b,c). Consistent with the ECM proteome analysis, mRNA expression profiles of CTIRPs, IRPs and DRPs further strengthen the finding that CTI, ROS and oligosaccharide signaling might prevent *Fusarium* invasion in C+F+ JG-62 seedlings. Moreover, eATP signaling appeared to play a significant role in chitosan-induced wilt resistance in the otherwise wilt-susceptible JG-62.

Mapping the quantitative ECM proteome onto the chitosan-regulated functional network

To determine the functional interaction associated with oligosaccharide signaling, CTI and eATP signaling components in C-F+ and C+F+ JG-62 during vascular wilt, we assembled protein abundance data and constructed a correlation network. The network was segregated into

modules of strongly co-expressed proteins showing variability in a time-dependent manner. Proteins belonging to proteases, wall biogenesis, disease response and redox homeostasis were found to be enriched in the DRP network of 61 nodes and 152 edges segregated into two large modules (Figure 5a–c). Module 1 (disease response), allied to 21 proteins, was enriched in oxidoreductases, proteases, hydrolases and dehydrogenases. Germin exhibited a maximum interaction with co-expressed proteins during fungal attack. A total of 34 proteins involved in wall biogenesis and redox homeostasis were mapped to module 2, with ascorbate peroxidase (APX) being the most interactive protein. Sub-functionalization of the disease network into two sub-networks, such as wall architecture remodeling (SN1; 41 nodes, 89 edges) and disease response (SN2; 24 nodes, 56 edges), provided information on how the ECM composition could be regulated during vascular fusariosis (Figure 5b,c).

The CTIRP network of 59 nodes and 123 edges consisted predominantly of proteins involved in oxidoreductase, protease and proteins acting on carbohydrate (Figure 5d–j). We distinguished two large modules and five small correlation groups, of which module 1 (oligosaccharide signaling) consisted of 14 proteins implicated in carbohydrate reorganization. Galactosidase appeared to be the most interactive CTIRP, demonstrating a significantly increased abundance at 240–480 hpi. CAZy, which is known to act as connecting link between oligosaccharide signaling to the immune response, exhibited increased abundance up to 480 hpi. Module 2 of 18 proteins was allied to redox homeostasis and eATP signaling, with purple acid phosphatase being the most interactive protein exhibiting inductive interaction. Next, we performed sub-functionalization of the chitosan-regulatory network into sub-networks and searched for additional ECM proteins that might dictate chitosan-triggered wilt resistance (Figure 5e–j). These sub-networks accounted considerably for CTIRPs linked to biological pathways involving glycan degradation (SN3; 13 nodes, 28 edges), hydration and acidification (SN4; 39 nodes, 82 edges), innate defense (SN5; 10 nodes, 21 edges), metal binding (SN6; 12 nodes, 27 edges), purine biogenesis (SN7; 10 nodes, 24 edges) and carbohydrate modification (SN8; 24 nodes, 54 edges). Sub-networks SN3 and SN8 were associated with oligosaccharide signaling and reorganization, indicating their involvement in stress-induced wall architecture remodeling. During stress conditions, macromolecule biogenesis plays a vital role in gene regulation. Our study revealed stress-induced upregulation of CAZymes but downregulation of fructose-bisphosphate aldolase in C+F+ JG-62. Sub-network SN4 connected to SN3 and SN8 was enriched in ROS machinery proteins. Peroxidase family members were upregulated while peroxidase was downregulated in C+F+ JG-62. Sub-networks SN3–SN5 were enriched in purple acid phosphatase,



GTP-binding proteins, pathogenesis-related proteins, resistance proteins and metal-binding proteins. These findings are indicative of stress-induced radical reprogramming for

activation of defense pathways. Co-regulation and interaction of CTIRPs, IRPs and DRPs suggested modulation of signal transduction pathways and a plethora of shared or

Figure 5. Protein network analysis. Network was constructed using protein expression data of studied conditions.

(a, d) Changes in expression profiles at different time points from two cultivars were captured in co-expression network. Each node represents a given protein based on top BLAST hit against SwissProt, and an edge denotes a probability of two given proteins (nodes) potentially interacting based on the cytoprophet algorithm. Protein sub-networks associated with patho-stress.

(b) Wall architecture remodeling.

(c) Disease response.

(e) Glycan degradation.

(f) Hydration and acidification.

(g) Innate defense.

(h) Metal binding.

(i) Purine biogenesis.

(j) Carbohydrate modification. Nodes and edges represent proteins and co-expression between proteins, respectively.

unique biological processes in C–F+ and C+F+ JG-62 and WR3-15 seedlings.

Chitosan evokes CTI by modulating ROS and NO production

To further confirm our observations of the morpho-histology, metabolome and ECM proteome concerning chitosan-induced ROS signaling, we examined ROS production in C–F+ and C+F+ JG-62 and C–F+ and C+F+ WR-315. Similar to C–F+ and C+F+ WR-315, C+F+ JG-62 exhibited pronounced ROS production up to 480 hpi (Figure 6a,b; Ashraf *et al.*, 2018). Next, we measured the time-dependent antioxidant enzyme activities of APX, SOD, lipoxygenase (LOX), diamine oxidase (DAO), glutathione peroxidase (GPX) and GR in four different datasets. Increased activities of these enzymes were indicative of resistance against *Fusarium* attack (Figure 6c–h). Matrix peroxidases and DAO have previously been shown to be the first component of the redox homeostasis machinery in the prevention of pathogen attack (Lamb and Dixon, 1997). Interestingly, compared with C–F+ JG-62, APX, LOX and DAO exhibited a progressive increase in activity up to 480 hpi in C–F+ and C+F+ WR-315 and C+F+ JG-62. However, SOD and GPX showed a sudden increase at 480 hpi, indicating a differential influence of antioxidant enzymes on ROS production during different phases of pathogen attack in C–F+ and C+F+ WR-315 and C+F+ JG-62 (Figure 6c–h). SOD is known to be the main determinant of the scavenging machinery for superoxide anion radicals. Thus, an increase in SOD activity should degrade superoxide radicals in C+F+ JG-62. The third response in C–F+ and C+F+ WR-315 and C+F+ JG-62 consisted of a considerable increase in GR activity (Figure 6h). Glutathione highly influences several H₂O₂ scavenging mechanisms either directly or indirectly. Thus, an increase in GR activity leads to a further reduction in the ROS concentration. The cooperative increase in GR and APX, two key enzymes in the ascorbate–glutathione cycle for H₂O₂ detoxification (Asada, 1992), clearly pointed to an intricate relation to CTI. The increased LOX activity might contribute to wilt resistance by generating either lipid hydroperoxides or defense-related gene

activation (Montillet *et al.*, 2005). In addition to ROS, rapid production of NO had been implicated in diverse physiological processes, including PCD and immunity (Yoshioka *et al.*, 2011). Estimation of the NO level by two independent methods in C+F+ JG-62 showed an increased NO burst (62–65%) up to 480 hpi (Figure 6i,j). We concluded that the interplay of ROS and NO evoked CTI during wilt resistance in chitosan-treated chickpea in response to *Fusarium*.

Chitosan-induced ROS and NO govern eATP signaling linked to stomatal function during *Fusarium* attack

To evaluate whether ROS and NO were accompanied by purinergic signaling mediated by extracellular ATP (eATP), we estimated the eATP concentration in four different datasets. Our results provide independent confirmation of the enhanced eATP levels (threefold increase) in a temporal manner (Figure 6k). It is known that eATP influences guard cell signaling pathways. With this aspect in mind, we investigated stomatal mechanics in leaf epidermal tissues of four different conditions (Figure 7a,b). Microscopic imaging revealed that the stomatal aperture decreased up to 120 hpi to prevent fungal penetration, followed by an increase in stomatal aperture up to 480 hpi to maintain transpiration in C–F+ and C+F+ WR-315 and C+F+ JG-62. We then measured stomatal physiological traits such as the transpiration rate and stomatal conductance (Figure 7c–e). C+F+ JG-62 seedlings exhibited a decreased transpiration rate and stomatal conductance up to 120 hpi, followed by a significant increase up to 480 hpi inducing stomatal opening or closure in a temporal manner, suggesting the presence of stomatal immunity associated with CTI.

DISCUSSION

Oligosaccharide elicitors such as chitosan have received considerable attention as key signaling molecules and positive modulators of the plant defense response. In rice and soybean, chitooctamer elicits diverse immune and allied cellular responses (Stacey and Shibuya, 1997; Shibuya and Minami, 2001). Chitosan oligomers are known to act as novel elicitors exhibiting antifungal properties against *Botrytis cinerea* in *Arabidopsis* and blister blight disease in

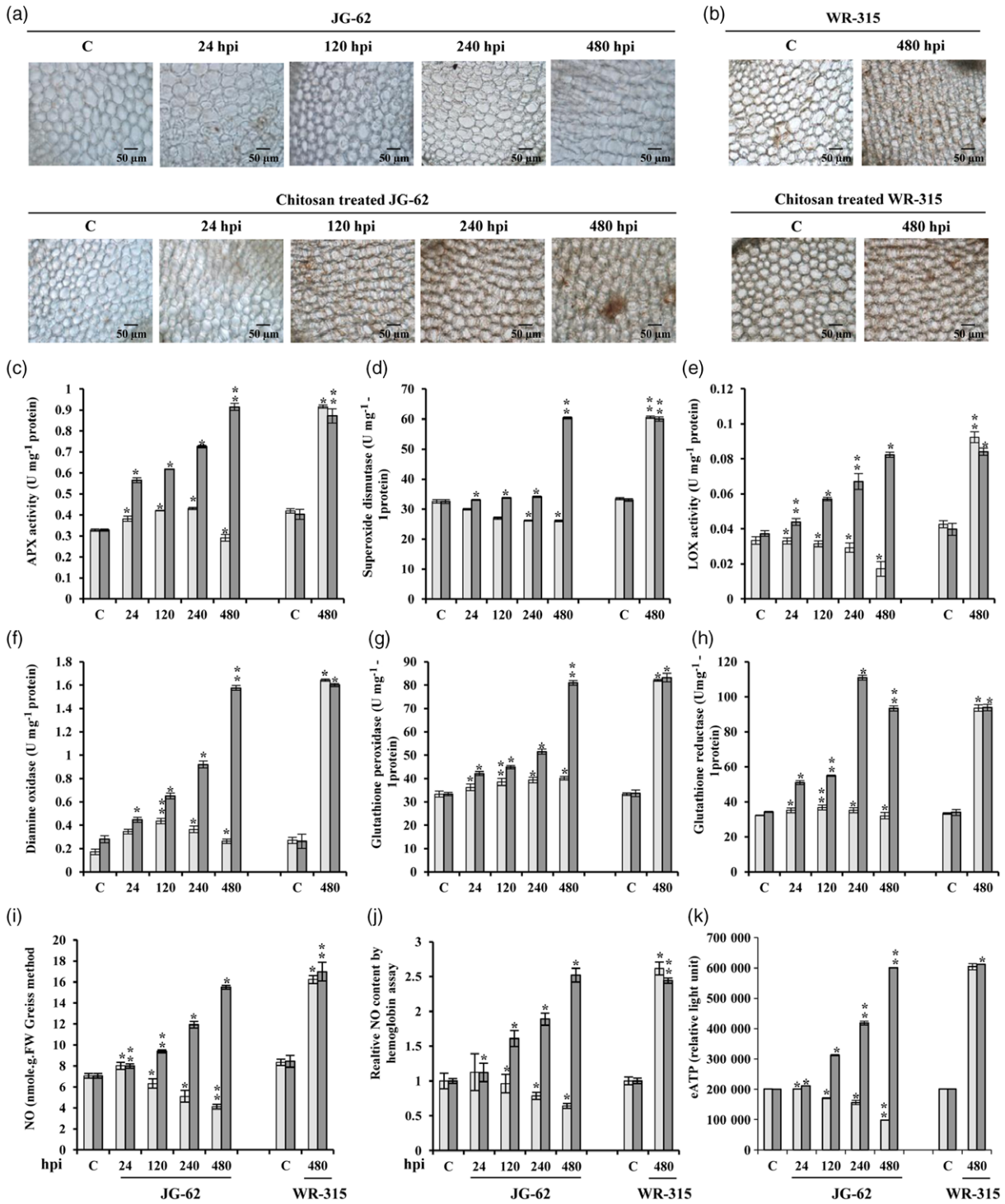


Figure 6. Reactive oxygen species (ROS) production and progression of *Fusarium oxysporum*. (a) Untreated and chitosan-treated JG-62 seedlings. (b) Without and with chitosan-treated WR-315 seedlings. (c) Estimation of ascorbate peroxidase (APX), (d) superoxide dismutase (SOD), (e) lipoxygenase (LOX), (f) diamine oxidase (DAO), (g) glutathione peroxidase (GPX), (h) glutathione reductase (GR). Changes were analyzed by ANOVA. Bars denote the mean values \pm SE. (i, j) Determination of NO levels. (k) Relative quantification of the extracellular (e)ATP concentration. Relative light unit (RLU) values represent the mean \pm SD, $n = 50$ (biological replicates). Changes were analyzed by ANOVA with $P < 0.01$. This experiment was repeated three times with similar results. Black bar denotes that seedlings were treated with chitosan, and gray bar represents seedlings without chitosan treatment. *Indicates statistical significance at $P < 0.05$.

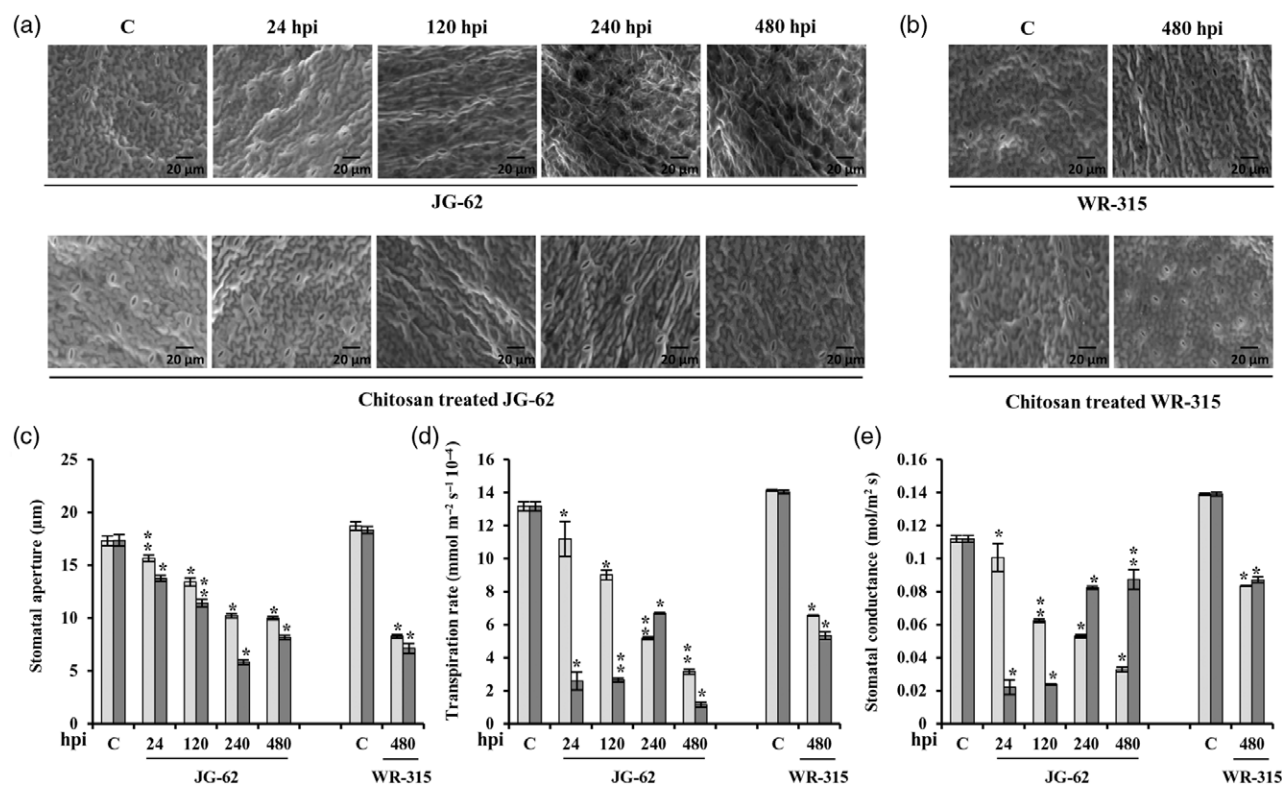


Figure 7. Influence of chitosan on stomatal function.

(a,b) Scanning electron micrographs (SEMs) illustrating opening and closing of stomata in untreated and chitosan-treated JG-62 leaves, and without and with chitosan-treated WR-315 leaves in response to *Fusarium*.

(c) Determination of stomatal aperture.

(d) Transpiration rate.

(e) Stomatal conductance across time points. The presented values represent \pm SD compared with the control (C). Black bar denotes chitosan-treated seedlings, and gray bar represents seedlings without chitosan treatment. *Indicates statistical significance at $P < 0.05$.

Camellia sinensis O. Kuntze against *Mycosphaerella graminicola* (Feng *et al.*, 2015; Chandra *et al.*, 2017). An antifungal property of chitosan has also been reported against *Ceratocystis fimbriata* in sweet potato (Xing *et al.*, 2018). The duration and concentration of chitosan pre-treatment play important roles in viral defense (Jia *et al.*, 2016). It is known that chitosan is a bioregulator and exhibits a potential metabolic response mechanism during plant growth (Zhang *et al.*, 2018). Chitosan mediates the feedback regulation of oligosaccharide signaling (Shibuya and Minami, 2001), and changes in the proteome have been shown to be part of the chitosan response in *Arabidopsis* (Ndimba *et al.*, 2003). Receptor-mediated activation of defense-related genes/gene-products is also known in PTI and ETI (Bigeard *et al.*, 2015). However, the initial perception, consequent signaling pathways and biological responses implicated in CTI remain largely unclear. Chitosan influences diverse biological processes and is thus expected to affect the immune status of plants. Currently, there has been a concerted effort to reduce fusariosis in crop plants. In this context, we compared the morpho-histological, biochemical, ECM proteome and metabolite

profiles of C-F+ and C+F+ wilt-susceptible and wilt-resistant chickpea genotypes, and conclusively demonstrated that the C+F+ wilt-susceptible cultivar exhibited temporal wilt resistance mediated by NO and ROS. Another interesting observation was formation of the root nodule, secondary root development and ECM fortification in C+F+ JG-62, revealing that the maintenance of water status and prevention of fungal penetration and colonization dictated wilt resistance. Chitosan is known to induce wall lignification and acidification, callose and ROS formation, ion fluxes, membrane depolarization, protein phosphorylation, phytoalexin biosynthesis, chitinase and the expression of early activation of defense-responsive proteins (El Hadrami *et al.*, 2010). We obtained similar results and hypothesized that these responses could be linked to carbohydrate reorganization-mediated ECM ultrastructural changes during fusariosis. Indeed, Raman spectroscopy, direct carbohydrate measurement and metabolite profiling revealed increased amounts of dynamic polysaccharide carbohydrate components (cellulose, pectin and lignin) with concomitant increases in osmoprotectants (trehalose, glycerol, proline and xylitol) in C+F+ wilt-susceptible genotype.

It was previously believed that chitosan/chitin induces the defense response through an uncharacterized signaling pathway. Thereafter, Wan *et al.* (2004) demonstrated that the chitin octamer mediated activation of a MAPK cascade in *Arabidopsis*. Very recently, it has been reported that classical salicylic acid, jasmonic acid or ethylene-responsive defense pathways do not suffice to activate chitin-elicited MAPK modules (Zhang *et al.*, 2018). However, the function of the ECM in chitosan-induced fungal resistance has not been elucidated. It is also unclear why some defense-associated proteins and metabolites are induced and other genes repressed by chitosan treatment. To address this issue, we developed a chitosan-responsive quantitative ECM proteome and metabolome of wilt-susceptible and wilt-resistant chickpea cultivars, and compared them with the respective chitosan untreated cultivars during fusariosis. These investigations involving different datasets revealed a subset of disease/immune-responsive ECM proteins responding to chitosan. The mRNA expression of 23 overlapping wall proteins obtained from different datasets in response to *Fusarium* infection was examined. In total, 12 common CTIRPs, IRPs and DRPs were linked to oligosaccharide signaling, while the remaining were associated with redox homeostasis, purinergic signaling and innate immunity. The increased abundance of chitinases (gi|5444006, gi|502131776, gi|502087868, gi|502154162), disease-resistance response proteins (gi|502147529, gi|502147532, gi|502084966, gi|502109348) and LysM domain-containing GPI-anchored protein (gi|502141811) in C–F+ WR-315 and C+F+ JG-62 compared with C–F+ JG-62 provided an important clue that oligosaccharide signaling initiated CTI against fungal disease in plants. A plethora of CAZymes and wall remodelers were enriched in the ECM proteome dataset, along with proteins interacting with carbohydrate and lipid metabolic pathway proteins. Furthermore, many CTIRPs associated with redox homeostasis showed an increased abundance in C–F+ WR-315 and C+F+ JG-62, and decreased abundance in C–F+ JG-62 during fusariosis. The role of purple acid phosphatases is well documented in eNTP utilization during the defense response (Liu *et al.*, 2016). We also observed an increased abundance of purple acid phosphatase isoforms (gi|502143528, gi|502154869, gi|502176175, gi|

502130502), indicating the possibility of extracellular dNTP involvement in CTI. Members of the peroxidase family have been postulated to be involved in the early defense response (Mohamed *et al.*, 2013), suggesting that peroxidase 21, 73 and 115 (gi|502129543, gi|502077140 and gi|5021334017) may be involved in the initial CTI signaling.

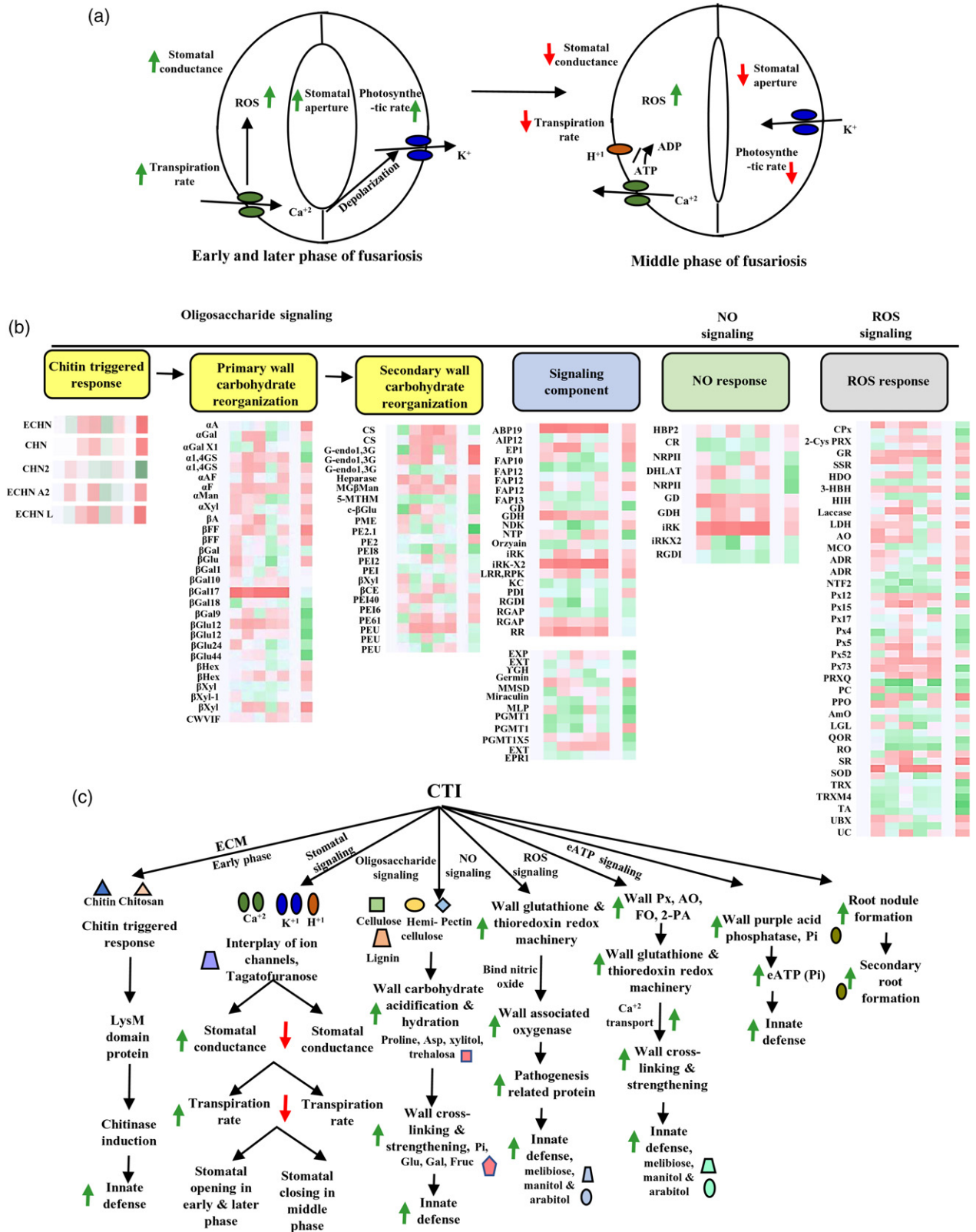
One of the major attributes of oligosaccharide elicitors, in contrast to other elicitors, is that they never induce the hypersensitive reaction (HR) leading to cell death. Rather, oligosaccharide elicitors regulate the ROS machinery and energy assimilation in plant defense (Tonón *et al.*, 2010). In *Arabidopsis*, NO and ROS production have been shown to be induced by extracellular nucleotides and to serve an important role in stomatal movement in response to stressors (Neill *et al.*, 2008; Tonón *et al.*, 2010). Further, eATP induces a variety of biological responses in both plants and animals. Some responses appear to be similar in both systems, including increased free calcium, NO and ROS (Tanaka *et al.*, 2010a,b). In plants, changes in the concentration of eATP have been observed in response to DAMP, chitin and yeast extract elicitors (Kim *et al.*, 2006; Wu *et al.*, 2008; Tanaka *et al.*, 2014). Additionally, the interplay of NO, ROS and eATP is well established in plant growth and development (Demidchik *et al.*, 2011; Soliman and El-Mohamedy, 2017). Extracellular nucleotides induce root hair growth stimulation and inhibition mediated by NO and ROS (Clark *et al.*, 2010). Given these considerations, we asked the following questions: do apoplast or guard cells release eATP? Does any interplay occur between ROS, NO and eATP during CTI? To address these questions, we measured ROS, antioxidant enzymes, NO and eATP. The results conclusively proved that increased ROS production and the subsequent induction of antioxidant enzymes and NO drive the release of eATP and the formation of secondary roots and root nodules during *Fusarium* attack. The molecular interplay of these signaling components dictates stomatal behavior to restrict pathogen entry. Our main findings illustrate that chitosan regulates ECM dynamics, stomatal function and root architecture. Overall, cell wall integrity signaling and stomatal immunity play pivotal roles in CTI and plant defense (Figure 8).

Figure 8. Mechanistic detail of chitosan-triggered immunity (CTI) during fusariosis.

(a) Schematic representation depicting changes in stomata during early, middle and later phase of fungal attack.

(b) Events associated with extracellular matrix (ECM) of chitosan-treated JG-62 seedlings challenged with *Fusarium oxysporum* compared with without treated WR-315 association. Proteins identified in this study are indicated in heat maps related to specific function.

(c) A model summarizing the events associated with chitosan-induced innate immunity in JG-62 seedlings challenged with *F. oxysporum*. Abbreviations: ECHN, endochitinase; CHN, chitinase; GAPDH, glyceraldehyde 3-P dehydrogenase; MDH, malate dehydrogenase; PP, inorganic pyrophosphatase; CCR, cinnamoyl CoA reductase-like 1; MHAR, monodehydroascorbate reductase; Prx, peroxiredoxin; PE, pectinesterase; PGK, phosphoglycerate kinase; AP, ascorbate peroxidase; LAP, lactoylglutathione lyase; ACC, 1-aminocyclopropane-1-carboxylate oxidase; AHC, adenosylhomocysteinase; Ser/thr P, serine/threonine phosphatase family protein; ROS, reactive oxygen species; α A, alpha arabinose; α Gal, alpha galactose; α 1,4 GS, alpha 1,4 glucan synthase; α Man, alpha mannosidase; α Xyl, alpha xylosidase; β FF, beta fructofuranosidase; β Glu, beta glucosidase; β Hex, beta hexosidase.



EXPERIMENTAL PROCEDURES

Plant material, chitosan and fungal treatment, and pathogenicity assay

Fusarium oxysporum f. sp. *ciceris* Race 1 (Foc1) was cultured without chitosan and with chitosan at increasing concentrations from 0.1 to 0.6 mg L⁻¹ for 10 days in PDA at 25°C. Surface-sterilized wilt-susceptible (JG-62) and wilt-resistant (WR-315) chickpea (*Cicer arietinum*, L) seeds treated with 0.6 mg L⁻¹ chitosan at room temperature. Seedlings were allowed to grow on MS basal agar medium (0.6% w/w) under 16 h/8 h (light/dark) photoperiod with 50 ± 5% relative humidity at 25 ± 2°C. Three-week-old seedlings were treated with either *Fusarium* spore suspension (1 × 10⁶/ml) grown in potato dextrose broth for 7 days at 28°C and 200 rpm or water as control. Both control and infected plants from chitosan-treated and untreated JG-62 and WR-315 seedlings were grown under the same conditions. Photographs of seedlings were taken at different time points followed by scoring of symptoms and disease severity. Chitosan-treated and untreated JG-62 seedlings infected with *Fusarium* were harvested at 6, 24, 120, 240 and 480 hpi. Chitosan-treated and untreated WR-315 challenged with *Fusarium* was harvested at 480 hpi. Mock inoculation with water was also performed, and samples were pooled to normalize the growth and developmental effects. All the samples were frozen in liquid nitrogen and stored at -80°C. Experiments were repeated three times for three independent biological replicates each consisting of 15 seedlings.

Fusarium oxysporum DNA extraction and quantification

Extraction of genomic DNA was performed from samples using DNeasy Plant Mini Kit (Qiagen, Germantown, MD, USA). *Fusarium* and chickpea specific gene primers and 20 ng of genomic DNA template for each sample were used for real-time PCR (RT-PCR) analyses, and the normalized Ct values were used to estimate fungal biomass. Primers spanning internal transcribed sequences of *F. oxysporum* gene were used to amplify and quantify fungal DNA. The sequence of the primers is listed in Table S3.

Physiological and biochemical analyses

Analyses were performed to measure RWC from dry weight (DW), fresh weight (FW) and turgid weight (TW), and ions leaching into the MQ water were recorded by measuring conductivity to estimate electrolyte leakage from the leaf sections. Free proline content and lipid peroxidation were measured for each sample as described earlier (Ashraf *et al.*, 2018). Experiments were performed for control and fungal-infected chitosan-treated and untreated JG-62 at 6, 24, 120, 240 and 480 hpi and WR-315 at 480 hpi. Four independent experiments were performed with three biological replicates each consisting of five plants. Vertical bars represent means of 12 biological replicates. Error bars indicate SD of mean ($n = 12$).

Scanning electron microscopy

For microscopic examination, 1–2 mm collar region of untreated and chitosan-treated chickpea seedlings challenged with *Fusarium* were fixed with 2.5% (v/v) glutaraldehyde, vacuumed three times and fixed for at least 24 h. Samples were dried, gold coated and observed under scanning electron microscope (SEM). Analysis was conducted and images were taken from three biological replications of the mounted specimens at bar, 20 µm. All procedures were performed based on the manufacturer's protocol.

Raman spectroscopy

Raman spectra of leaves were obtained using an imaging spectrometer. CW laser at 532 nm and 10 mW laser power was focused to excite the spectra. Spectra were accumulated for 1 sec, frequency calibrated using spectrum of toluene and spikes were removed, and Raman scattering was collected with confocal illumination. Spectral resolution was 3–4 cm⁻¹ in the full spectral range. Raman spectra analysis was performed using WITTEC Project FOUR software.

Plant ECM fractionation and estimation of cellulose, pectin and lignin

The ECM and polysaccharides were extracted as described by Peng (2000) with minor modifications. Samples were dried at 65°C until a constant weight was achieved followed by mechanical crushing using mortar pestle. To remove soluble sugars, lipids and starch, 0.1 g samples were treated with potassium phosphate buffer (pH 7.0), chloroform:methanol (1:1, v/v) and dimethylsulfoxide (DMSO):water (9:1, v/v) for 4.5 h. The crude ECM extract was suspended in 0.5% (w/v) ammonium oxalate, boiled for 1 h in a water bath and the supernatants were collected as total pectin. Pellet was dissolved in 4 M KOH containing 1.0 mg ml⁻¹ sodium borohydride for 1 h at 25°C, and centrifuged at 10 000 g for 10 min. Supernatant was neutralized, dialyzed and lyophilized as hemicelluloses. The KOH non-extractable residue was further boiled in acetic acid:nitric acid:water (8:1:2, v/v/v) for 1 h with constant stirring every 10 min at 100°C followed by cooling at room temperature. Extract was centrifuged at 10 000 g for 10 min. After several washes in 5 ml water, pellets were dissolved in 67% H₂SO₄ to obtain cellulose. Total lignin was determined by two-step acid hydrolysis method as described in Laboratory Analytical Procedure of the National Renewable Energy Laboratory (Sluiter *et al.*, 2008; Wu *et al.*, 2008). Four independent experiments were performed with three biological replicates each consisting of five plants. Vertical bars represent means of 12 replicates. Error bars indicate SD of mean ($n = 12$).

Metabolite profiling by GC-MS analysis

For metabolite analyses, untreated and chitosan-treated WR-315 and JG-62 seedlings were challenged without (control) or with fungal inoculum up to 480 hpi. Seedlings were harvested and stored as described above. Extraction and derivatization of metabolites were performed according to Schauer *et al.* (2005). Briefly, 200 mg seedlings were homogenized in 1400 µl 100% methanol containing 50 µl ribitol as internal standard (2 mg ml⁻¹) followed by extraction for 15 min at 70°C, dilution in 1 vol water, centrifugation at 2200 g and drying of supernatant *in vacuo* for 9–16 h. Derivatization and treatment of dried residue was performed in 80 µl of methoxyamine hydrochloride (20 mg ml⁻¹) for 90 min at 30°C and 80 µl MSTFA for 30 min at 37°C. Prior to trimethylsilylation, 40 µl of retention time standard mixture was added and derivatized extracts were diluted 10-fold in *n*-heptane; 1 µl diluted derivatized extract was injected in splitless mode into Shimadzu GCMSQP 2010 plus. For performing GC, Rtx5MS-30 m column with 0.25 mm I.D. and df 0.25 (Restek) was used. Injection, interface and ion source temperatures were set at 260°C, 270°C, 230°C, respectively, and helium was used as the carrier gas at a flow rate of 1 ml min⁻¹. The analysis was performed as described in Schauer *et al.* (2005). Tuning of mass spectrometer was done and mass spectra were recorded at 2 scan sec⁻¹ with m/z 40–600 scanning range followed by peak assignment and quantification. To allow comparison between the samples, data normalization was

performed based on the mean response for the control of each replicate as per Ghosh *et al.* (2016). Metabolites were identified by comparing retention times, m/z and mass spectra of each compound against a standard mass chromatogram in the NIST or WILEY library. Compounds with significant changes ($P < 0.05$) and fold change > 2 were subjected to Metaboanalyst for pathway impact analysis. Experiments were performed in four replicates each consisting of five plants.

ECM isolation and protein extraction

Isolation and purification of ECM fraction was carried out as described by Bhushan *et al.* (2006). ECM fraction was obtained by grinding 15 g seedling tissue in liquid nitrogen with 0.3% (w/w) polyvinylpyrrolidone (PVPP) followed by homogenization in 5 mM K_3PO_4 , pH 6.0, 5 mM dithiothreitol (DTT), 1 mM PMSF for 2 min. Extract was centrifuged at 1000 *g* for 5 min at 4°C and pellet was washed 10 times with water. The purity of ECM fraction was evaluated by transmission electron microscopy and organelle-specific marker enzyme assays as described earlier (Elagamey *et al.*, 2017a,b).

Extracellular matrix (ECM) proteins were extracted from ECM fraction by suspending washed pellets in three volumes (w/v) of extraction buffer [200 mM $CaCl_2$, 5 mM DTT, 1 mM PMSF, 0.3% (w/w) PVPP] kept on shaker for 2 h. Proteins were separated, filtered, concentrated and dialyzed overnight against 1000 volumes of deionized water and diluted as described by Elagamey *et al.* (2017a). Diluted proteins were boiled for 5 min, centrifuged at 10 000 *g* for 10 min at 4°C, pellets were washed twice with 80% acetone and air-dried. Dried pellets were dissolved in 50 μ l dissolution buffer [0.5 M triethylammonium bicarbonate (TEAB), pH 8.5], centrifuged at 13 000 *g* for 10 min, reduced with 4 μ l reagent, and incubated at 60°C for 1 h. Then 2 μ l cysteine blocking reagent was added at room temperature for 10 min according to the manufacturer's instructions (AB Sciex, Redwood City, CA, USA). Protein concentration was determined using the Bradford protein assay (Bio-Rad protein assay kit, Hercules, CA, USA).

Trypsin digestion and iTRAQ labeling

After ECM protein extraction, 75 μ g of protein in 0.5 M TEAB was digested overnight with 5.5 μ g trypsin at 37°C. Each peptide digest was dried in a SpeedVac, resuspended in 30 μ l 0.5 M TEAB and labeled for 3 h at room temperature using iTRAQ 8-plex kit by adding one reagent vial of an isobaric tag to each peptide sample according to the manufacturer's manual (AB Sciex, USA). The control sample of chitosan-treated JG-62 was labeled with iTRAQ tag 114, and without chitosan-treated WR-315 (control) was tagged with 119. *Fusarium* challenged chitosan-treated JG-62 seedlings were labeled with tags 113, 115, 116, 117 and 118 for 6, 24, 120, 240, 480 hpi, respectively. However, without chitosan-treated WR-315 seedlings challenged with *Fusarium* at 480 hpi were tagged with 121. Similarly, control sample of C-F+ JG-62 seedlings was labeled with iTRAQ tag 114 and tags 113, 115, 116, 117, 118, 119, 121 for 0.5, 6, 12, 24, 48, 72, 120 hpi, respectively. Two separate iTRAQ labeling kits were used for C+F+ and C-F+ datasets. Excess iTRAQ reagent was quenched with water, the samples were then combined, desalted on a Strata-X 33 μ m polymeric reverse phase column (Phenomenex, Torrance, CA, USA) and dried. Experiments were performed in three replicates each consisting of 15 seedlings. Peptides were fractionated by strong cation exchange chromatography on an Agilent 1100 HPLC system (Agilent Technologies, Palo Alto, CA, USA) using a PolySulfoethyl column (4.6–100 mm, 5 μ m, 300 Å) and eluted with a linear

gradient of Buffer B (1 M KCl, 10% ACN and 10 mM KH_2PO_4 , pH 3.0). A total of 40 fractions were collected and pooled into eight fractions, desalted and dried before mass spectrometry analysis.

Reverse-phase nanoflow HPLC and tandem mass spectrometry

Following SCX fractionation, 1.0–1.8 μ g of each fraction was injected into an Agilent Zorbax 300SB C18, 3.5 μ m (Agilent Technologies) in Shimadzu Prominence nano HPLC system (Shimadzu, Kyoto, Japan). Peptides were resolved with a gradient of 10–40% acetonitrile (0.1% trifluoroacetic acid) over 160 min and analyzed on a TripleTOF 5600 mass spectrometer (AB Sciex). Data were acquired using an ion spray voltage of 2.3 kV, curtain gas of 25, nebulizer gas of 20, and an interface heater temperature of 150°C. The MS was operated with a resolution of 30 000 fwhm for TOF MS scans. For IDA, survey scans were acquired in 250 msec, and 35 product ion scans were collected if they exceeded a threshold of 150 counts sec^{-1} with a +2 to +5 charge state. Total cycle time was 2.5 sec and dynamic exclusion set to 18 sec. A rolling collision energy setting was applied to precursor ions for collision-induced dissociation.

Protein identification and quantification

The MS/MS data were analyzed using ProteinPilot Software 4.0 (AB Sciex, USA) against the viridiplantae (75925788 sequences; 27045014025 residues) and *F. oxysporum* database, and the FDR was estimated using integrated PSPEP tool. Search parameters included iTRAQ 8-plex quantification, carbamidomethyl modification of cysteine residues, trypsin digestion and protein threshold of 95% confidence (unused protein score > 1.3). The screening criteria for CTIRPs, IRPs and DRPs included a fold change > 1.5 or < 0.67 and $P < 0.05$ based on quantitative information from at least three independent peptides in each replicate, FDR $\leq 1\%$ and a unique peptide ≥ 1 based on protein abundance and comparison among groups. Only the significant ratios among the replicates were used to calculate average protein ratio. Proteins with CI 95% were evaluated based on number of peptides matched, MOWSE score, % coverage, similarity of theoretical and experimental molecular masses. Differentially expressed proteins were identified and quantified with at least three unique peptides. Protein functions were assigned using Pfam or InterPro. Functional annotation of the proteins was conducted using KEGG (<http://www.genome.jp/kegg/>), COG (<http://www.ncbi.nlm.nih.gov/COG/>) and Blast2GO (<https://www.blast2go.com/>) against the NCBI non-redundant protein database.

Statistical analysis

K-means clustering analysis of CTIRPs, IRPs, DRPs that showed altered expression in at least one time point was performed by MeV software (TIGR). Expression values of the individual protein measured were used to identify the similarity and differences in expression pattern between samples. PCA, volcano plot and two-way ANOVA were performed on CTIRPs, IRPs, DRPs using XLSTAT. PCA parameters included SAMPLE SELECTION as Cluster genes and CENTERING MODE as mean.

Real-time PCR

Quantitative real-time PCR was performed to validate RNA expression profiles of few CTIRPs, IRPs, DRPs selected from the differential ECM proteome datasets. Total RNA quantification was done on a NanoDrop Spectrophotometer (Nanodrop Technologies, Wilmington, DE, USA). cDNA was synthesized from

5 µg of total RNA using reverse transcriptase kit (Applied Biosystems, Waltham, MA, USA) and diluted 10 times. The reaction mixture was prepared for individual genes in triplicate using SYBR Green Master Mix (Applied Biosystems). PCR was performed on an ABI 7500 sequence detection system according to the manufacturer's protocol (Applied Biosystems). Relative gene expression values were normalized with expression of the reference gene 18S using the $\Delta\Delta C_t$ method. Primer sequences are listed in Table S3.

Protein correlation network

Protein–protein interactions (PPIs) were searched against databases and visualized with Cytoscape version 3.0.2 (Shannon *et al.*, 2003) using Prefuse Force Directed Layout as described in Ghosh *et al.* (2016). PPIs of non-redundant CTIRPs, IRPs, DRPs were predicted in this analysis.

DAB staining

Roots of untreated and chitosan-treated seedlings challenged with *F. oxysporum* were stained in 1 mg ml⁻¹ of 3,3'-diaminobenzidine (DAB) buffer and kept for 10 h at RT. Samples were boiled in acetic acid and lactophenol for 2 min followed by rinsing in 50% ethanol five times, and roots were observed under Nikon Eclipse 80i Microscope (Nikon, Tokyo, Japan).

Antioxidant enzyme activities and NO measurement

Ascorbate peroxidase, CAT, GPX, GR, SOD and DAO were assayed, and their units of activity were defined as previously described (Garcia-Limonos *et al.*, 2002). Protein concentration was determined by Bradford assay with bovine serum albumin as standard. Spectrophotometric data are means of four independent experiments with three biological replicates each consisting of five plants. Vertical bars represent means of 12 biological replicates. Error bars indicate SD of mean ($n = 12$). The significant differences between means were determined by Student's *t*-test at $P < 0.05$.

Griess Assay was performed to determine NO level. An equal volume of Griess reagent [1% sulfanilamide and 0.1% *n*-(1-naphthyl) ethylenediamine dihydrochloride in 5% H₃PO₄; Sigma, St Louis, MO, USA] was added to the samples and incubated for 10 min at room temperature. Absorbance was recorded in a spectrophotometer at 570 nm. The standard curve for NO²⁻ concentration was determined using NaNO₂ dissolved in DMEM as a standard and DMEM alone as a blank. Spectrophotometric data are means of four independent experiments with three biological replicates each consisting of five plants. Vertical bars represent means of 12 biological replicates. Error bars indicate SD of mean ($n = 12$). The significant differences between means were determined by Student's *t*-test at $P < 0.05$.

NO content was also measured by haemoglobin assay; 1 g of chickpea seedlings from four datasets was ground and homogenized in 0.1 M sodium acetate, 1 M NaCl and 1% (w/v) ascorbic acid, pH 6.0 as previously described (Shi *et al.*, 2012). Homogenates were centrifuged at 12 000 rpm for 20 min at 4°C. Supernatant was incubated with 100 U ml⁻¹ catalase (Sigma) and 100 U ml⁻¹ SOD (Sigma) for 5 min to remove ROS before adding HbO₂ (10 µM final concentration; haemoglobin-A0 human, Sigma). NO content was quantified spectrophotometrically by measuring conversion of oxyhaemoglobin to methaemoglobin at 401 and 421 nm, using an extinction coefficient of 77 mm⁻¹ cm⁻¹ (A₄₀₁ HbO₂-A₄₂₁ metHb; Murphy and Noack, 1994). Data are means of four independent experiments with three biological replicates

each consisting of five plants. Vertical bars represent means of 12 biological replicates. Error bars indicate SD of mean ($n = 12$). The significant differences between means were determined by Student's *t*-test at $P < 0.05$.

eATP determination

Leaves of untreated and chitosan-treated seedlings were incubated with 100 µg ml⁻¹ luciferase (Sigma, SRE0045) protein solution for 1 h at room temperature. *Fusarium oxysporum* was then added to the sample and incubated for 30 min at 23°C under light followed by washing three times with sterile ddH₂O. Subsequently, samples were treated with a flash assay buffer containing 20 mM Tris, 3 mM MgSO₄, 0.1 mM EDTA, 2 mM DTT and 500 µM D-luciferin (Sigma, L6882). Fluorescence was monitored using a Zeiss Axiovert 200M with Leica DFC290 color camera and DFC340 monochrome camera. Data are means of two independent experiments with three biological replicates each consisting of five plants. Vertical bars represent means of six biological replicates. Error bars indicate SD of mean ($n = 6$). The significant differences between means were determined by Student's *t*-test at $P < 0.05$.

Stomatal aperture, stomatal conductance and transpiration rate measurement

For whole leaf experiments, leaves were removed from untreated and chitosan-treated WR-315 and JG-62 seedlings challenged with *Fusarium* up to 480 hpi. For each treatment, about four peels collected from four different leaves of at least two plants were floated on 3 ml of leaf buffer consisting of 10 mM KCl, 25 mM MES, pH 6.15 with the abaxial side up in Petri dishes. Photographs of 70–90 stomata per treatment were taken, of which stomatal aperture width of 50 stomata were measured using the image processing software ImageJ. The ratio of closed stomata (width of 0) to open stomata was determined for all imaged stomata. Stomatal apertures were determined as width:length ratio. Statistical significance of the measurements for the treatments was determined using Student's *t*-test in Microsoft Excel.

Stomatal conductance and transpiration rate were measured with a portable photosynthesis measurement system (GFS3000; waltz). The photosynthetic capability of plants was recorded under standard atmospheric (360 ppm CO₂) and light conditions (750 µmol m⁻² sec⁻¹) based on single leaf measurements of five–seven different leaves of three plants. Leaves were held in the chamber for 2–3 min until the rates of transpiration and stomatal conductance were in a steady-state condition. Experiments were repeated thrice.

ACKNOWLEDGEMENTS

This work was supported by grants from Department of Biotechnology, Govt. of India (No. BT/PR10796/BRB/10/621/2008, BT/HRD/35/01/05/2013, BT/PR23748/BPA/118/345/2017 and BT/PR25260/NER/95/1102/2017) and National Institute of Plant Genome Research, New Delhi, India to S.C. E.E. is the recipient of post-doctoral fellowship from DBT-TWAS. M.A. was the recipient of post-doctoral fellowship from DBT-TWAS. K.N. is the recipient of post-doctoral fellowship from Department of Biotechnology (DBT), Govt. of India. Financial support from the DBT-RA program in Biotechnology and Life Sciences is gratefully acknowledged. A.S. is the recipient of pre-doctoral fellowship from the Council of Scientific and Industrial research (CSIR), Govt. of India. S.G. is the recipient of Science and Engineering Research Board (SERB), DST, Govt. of India. The authors also thank Mr

Jasbeer Singh for illustrations and graphical representations in the manuscript.

AUTHOR CONTRIBUTIONS

SC conceived the experiments; SC, KN and EE designed the experiments; EE, MA, KN and AS performed the experiments; KN, EE, SG, AS, MA, NC and SC analyzed the data; SC, KN and EE wrote the paper.

CONFLICT OF INTEREST

The authors declare that there is no conflict of interests regarding the publication of this manuscript.

DATA AVAILABILITY STATEMENT

Data supporting the findings of this work are accessible within the paper and its Supporting Information files. All other data generated and analyzed during the current study are available from the corresponding author upon reasonable request.

SUPPORTING INFORMATION

Additional Supporting Information may be found in the online version of this article.

Figure S1. Effect of chitosan on root nodule formation of chitosan-treated JG-62 in response to *Fusarium*. (a) Photograph showing changes in root architecture and formation of root nodules. (b) Estimation of RWC. (c) Determination of total proline content of C-F+ and C+F+ JG-62 and WR-315 seedlings. The presented values \pm SD are relative values compared with the control. *Indicates statistical significance $P < 0.05$. Black bar denotes that seedlings were treated with chitosan, and gray bar represents seedlings without chitosan treatment.

Figure S2. Functional enrichment of the DRPs, CTIRPs and IRPs. Distribution of DRPs, CTIRPs and IRPs based on Blast2GO analyses. Y-axis indicates significant Blast2GO functional categories ($P < 0.05$) and the X-axis shows number of proteins. (a) Molecular function. (b) Biological process.

Figure S3. Hierarchical clustering of CTIRPs and IRPs.

Figure S4. Hierarchical clustering of DRPs.

Figure S5. Comparison of protein abundance and mRNA levels. (a) Relationships between the 1.5-fold difference and statistical significance using *t*-test are presented by volcano plots for each time point (0.5, 12 and 48 hpi), the DRPs with the greatest significant difference are shown based on function as red (innate defense), green (redox homeostasis) and blue (carbohydrate reorganization). (b) Analysis of levels of proteins and mRNA. Relative quantification (RQ) of mRNA levels was performed on candidate DRPs by qRT-PCR. Expression changes were analyzed by ANOVA. (c) Box whisker plot showing the range of coverage of DRPs and respective mRNA within each time point.

Table S1. List of differential ECM proteins identified by mass spectrometric analysis.

(a) DRPs identified by MS/MS analysis. (b) CTIRPs identified by MS/MS analysis. (c) IRPs identified by MS/MS analysis.

Table S2. Domain analysis of unknown ECM proteins.

(a) DRPs with unknown function. (b) CTIRPs and IRPs with unknown function.

Table S3. Genes and primers used for qRT-PCR analysis.

REFERENCES

- Akamatsu, A., Wong, H.L., Fujiwara, M. *et al.* (2013) An OsCEBiP/OsCERK1-OsRacGEF1-OsRac1 module is an essential early component of chitin-induced rice immunity. *Cell Host Microbe* **13**, 465–476.
- Alburquenque, C., Bucarey, S.A., Neira-Carrillo, A., Urzúa, B., Hermosilla, G. and Tapia, C.V. (2010) Antifungal activity of low molecular weight chitosan against clinical isolates of *Candida* spp. *Med Mycol* **48**, 1018–1023.
- Amborabé, B.E., Bonmort, J., Fleurat-Lessard, P. and Roblin, G. (2008) Early events induced by chitosan on plant cells. *J. Exp. Bot.* **59**, 2317–2324.
- Ao, Y., Li, Z., Feng, D., Xiong, F., Liu, J., Li, J.F., Wang, M., Wang, J., Liu, B. and Wang, H.B. (2014) OsCERK1 and OsRLCK176 play important roles in peptidoglycan and chitin signaling in rice innate immunity. *Plant J.* **80**, 1072–1084.
- Asada, K. (1992) Ascorbate peroxidase: a hydrogen peroxide scavenging enzyme in plants. *Physiol. Plant* **85**, 235–241.
- Ashraf, N., Basu, S., Narula, K., Ghosh, S., Tayal, R., Gangisetty, N., Biswas, S., Aggarwal, P.R., Chakraborty, N. and Chakraborty, S. (2018) Integrative network analyses of wilt transcriptome in chickpea reveal genotype dependent regulatory hubs in immunity and susceptibility. *Sci. Rep.* **8**, 6528.
- Bandaranayake, P.C., Filappova, T., Tomilov, A., Tomilova, N.B., Jamison-McClung, D., Ngo, Q., Inoue, K. and Yoder, J.I. (2010) A single-electron reducing quinone oxidoreductase is necessary to induce haustorium development in the root parasitic plant *Triphysaria*. *Plant Cell* **22**, 1404–1419.
- Benhamou, N., Kloepper, J.W. and Tuzun, S. (1998) Induction of resistance against *Fusarium* wilt of tomato by combination of chitosan with an endophytic bacterial strain: ultrastructure and cytochemistry of the host response. *Planta* **204**, 153–168.
- Bhushan, D., Pandey, A., Chattopadhyay, A., Choudhary, M.K., Chakraborty, S., Datta, A. and Chakraborty, N. (2006) Extracellular matrix proteome of chickpea (*Cicer arietinum* L.) illustrates pathway abundance, novel protein functions and evolutionary perspective. *J. Proteome Res.* **5**, 1711–1720.
- Bigeard, J., Colcombet, J. and Hirt, H. (2015) Signaling mechanisms in pattern-triggered immunity (PTI). *Mol. Plant* **8**, 521–539.
- Chandra, S., Chakraborty, N., Panda, K. and Acharya, K. (2017) Chitosan-induced immunity in *Camellia sinensis* (L.) O. Kuntze against blister blight disease is mediated by nitric-oxide. *Plant Physiol. Biochem.* **115**, 298–307.
- Clark, G., Wu, M., Wat, N. *et al.* (2010) Both the stimulation and inhibition of root hair growth induced by extracellular nucleotides in *Arabidopsis* are mediated by nitric oxide and reactive oxygen species. *Plant Mol. Biol.* **74**, 423–435.
- Day, R.B., Okada, M., Ito, Y., Tsukada, K., Zaghouni, H., Shibuya, N. and Stacey, G. (2001) Binding site for chitin oligosaccharides in the soybean plasma membrane. *Plant Physiol.* **126**, 1162–1173.
- Demidchik, V., Shang, Z., Shin, R., Colaço, R., Laohavisit, A., Shabala, S. and Davies, J.M. (2011) Receptor-like activity evoked by extracellular ADP in *Arabidopsis* root epidermal plasma membrane. *Plant Physiol.* **156**, 1375–1385.
- Elagamey, E., Narula, K., Sinha, A., Ghosh, S., Abdellatif, M.A.E., Chakraborty, N. and Chakraborty, S. (2017a) Quantitative extracellular matrix proteomics suggests cell wall reprogramming in host-specific immunity during vascular wilt caused by *Fusarium oxysporum* in chickpea. *Proteomics* **17**, 23–24.
- Elagamey, E., Sinha, A., Narula, K., Abdellatif, M.A.E., Chakraborty, N. and Chakraborty, S. (2017b) Molecular dissection of extracellular matrix proteome reveals discrete mechanism regulating *Verticillium dahliae* triggered vascular wilt disease in potato. *Proteomics* **17**, 1600–1607.
- Faulkner, C., Petutschnig, E., Benitez-Alfonso, Y., Beck, M., Robatzek, S., Lipka, V. and Maule, A.J. (2013) LYM2-dependent chitin perception limits molecular flux via plasmodesmata. *Proc. Natl Acad. Sci. USA* **110**, 9166–9170.
- Feng, H., Xia, W., Shan, C., Zhou, T., Cai, W. and Zhang, W. (2015) Quaternized chitosan oligomers as novel elicitors inducing protection against *B. cinerea* in *Arabidopsis*. *Int. J. Biol. Macromol.* **72**, 364–369.
- Fliegmann, J., Uhlenbroich, S., Shinya, T., Martinez, Y., Lefebvre, B., Shibuya, N. and Bono, J.J. (2011) Biochemical and phylogenetic analysis of CEBiP-like LysM domain-containing extracellular proteins in higher plants. *Plant Physiol. Biochem.* **49**, 709–720.

- Fristsensky, B., Rigglesman, R.C., Wagoner, W. and Hadwiger, L.A. (1985) Gene expression in susceptible and disease resistant interactions of peas induced with *Fusarium solani* pathogens and chitosan. *Physiol. Plant Pathol.* **27**, 15–28.
- Furukawa, S., Taniyai, K., Yang, J., Shono, T. and Yamakawa, M. (1999) Induction of gene expression of antibacterial proteins by chitin oligomers in the silkworm, *Bombyx mori*. *Insect Mol. Biol.* **8**, 145–148.
- García-Limones, C., Hervás, A., Navas-Cortés, J.A., Jiménez-Díaz, R.M. and Tena, M. (2002) Induction of an antioxidant enzyme system and other oxidative stress markers associated with compatible and incompatible interactions between chickpea (*Cicer arietinum* L.) and *Fusarium oxysporum* f. sp. *ciceris*. *Physiol. Mol. Plant Pathol.* **61**, 325–337.
- Ghosh, S., Narula, K., Sinha, A., Ghosh, R., Jawa, P., Chakraborty, N. and Chakraborty, S. (2016) Proteometabolic analysis of transgenic tomato overexpressing oxalate decarboxylase uncovers novel proteins potentially involved in defense mechanism against *Sclerotinia*. *J. Proteomics* **143**, 242–253.
- Goya, R.C., Morais, S.T.B. and Assis, O.B.G. (2016) Evaluation of the antimicrobial activity of chitosan and its quaternized derivative on *E. coli* and *S. aureus* growth. *Rev. Bras. Farmacogn.* **26**, 122–127.
- Guo, M., Chen, K. and Zhang, P. (2012) Transcriptome profile analysis of resistance induced by burdock fructooligosaccharide in tobacco. *J. Plant Physiol.* **169**, 1511–1519.
- Gust, A.A., Willmann, R., Desaki, Y., Grabherr, H.M. and Nürnberger, T. (2012) Plant LysM proteins: modules mediating symbiosis and immunity. *Trends Plant Sci.* **17**, 495–502.
- El Hadrami, A., Adam, L.R., El Hadrami, I. and Daay, F. (2010) Chitosan in plant protection. *Mar. Drugs* **8**, 968–987.
- El Hassni, M., El Hadrami, A., Daayf, F., Chérif, M., Ait Barka, E. and El Hadrami, I. (2004) Chitosan, antifungal product against *Fusarium oxysporum* f. sp. *albedinisand* elicitor of defence reactions in date palm roots. *Phytopathol. Mediterr.* **43**, 195–204.
- Hadwiger, L.A. and Beckman, J.M. (1980) Chitosan as a Component of *Pea-Fusarium solani* Interactions. *Plant Physiol.* **66**, 205–211.
- Iriti, M. and Faoro, F. (2009) Chitosan as a MAMP, searching for a PRR. *Plant Signal Behav.* **4**, 66–68.
- Itoh, T., Hibi, T., Fujii, Y., Sugimoto, I., Fujiwara, A., Suzuki, F., Iwasaki, Y., Kim, J.K., Taketo, A. and Kimoto, H. (2013) Cooperative degradation of chitin by extracellular and cell surface-expressed chitinases from *Paenibacillus* sp. strain FPU-7. *Appl. Environ. Microbiol.* **79**, 7482–7490.
- Jia, X., Meng, Q., Zeng, H., Wang, W. and Yin, H. (2016) Chitosan oligosaccharide induces resistance to Tobacco mosaic virus in *Arabidopsis* via the salicylic acid-mediated signalling pathway. *Sci. Rep.* **6**, 26 144.
- Jiménez-Díaz, R.M., Trapero-Casas, A. and de la Colina, J.C. (1989) Races of *Fusarium Oxysporum* F. sp. *Ciceri* infecting chickpeas in Southern Spain. In *Vascular Wilt Diseases of Plants* (Tjamos, E.C. and Beckman, C.H., eds), NATO ASI Series (Series H: Cell Biology), Vol. 28. Berlin: Springer.
- Kaku, H., Shibuya, N., Xu, P., Aryan, A.P. and Fincher, G.B. (1997) N-acetylchitooligosaccharide elicitor expression of a single 1,3- β -glucanase gene in suspension-cultured cells from barley (*Hordeum vulgare*). *Physiol. Plant.* **100**, 111–118.
- Kim, S.Y., Sivaguru, M. and Stacey, G. (2006) Extracellular ATP in plants. Visualization, localization, and analysis of physiological significance in growth and signalling. *Plant Physiol.* **142**, 984–992.
- Koehle, H., Jeblick, W., Poten, F., Blaschek, W. and Kauss, H. (1985) Chitosan-elicited callose synthesis in soybean cells as a Ca²⁺-dependent process. *Plant Physiol.* **77**, 544–551.
- Lamb, C. and Dixon, R.A. (1997) The oxidative burst in plant disease resistance. *Annu. Rev. Plant Physiol. Plant Mol. Biol.* **48**, 251–275.
- Lee, W.S., Rudd, J.J., Hammond-Kosack, K.E. and Kanyuka, K. (2014) Mycosphaerella graminicola LysM effector-mediated stealth pathogenesis subverts recognition through both CERK1 and CEBIP homologues in wheat. *Mol. Plant Microbe Interact.* **27**, 236–243.
- Liu, P.D., Xue, Y.B., Chen, Z.J., Liu, G.D. and Tian, J. (2016) Characterization of purple acid phosphatases involved in extracellular dNTP utilization in *Stylosanthes*. *J. Exp. Bot.* **67**, 4141–4154.
- Meng, P.H., Raynaud, C., Tcherkez, G. et al. (2009) Crosstalks between myo-inositol metabolism, programmed cell death and basal immunity in *Arabidopsis*. *PLoS One* **4**, e7364.
- Mohamed, S.A., Al-Malki, A.L., Kumosani, T.A. and El-Shishtawy, R.M. (2013) Horseradish peroxidase and chitosan: activation, immobilization and comparative results. *Int. J. Biol. Macromol.* **60**, 295–300.
- Montillet, J.L., Chamnongpol, S., Rustérucci, C., Dat, J., van de Cotte, B., Agnel, J.P., Battesti, C., Inzé, D., Van Breusegem, F. and Triantaphylidès, C. (2005) Fatty acid hydroperoxides and H₂O₂ in the execution of hypersensitive cell death in tobacco leaves. *Plant Physiol.* **138**, 1516–1526.
- Murphy, M.E. and Noack, E. (1994) Nitric oxide assay using haemoglobin method. *Methods Enzymol.* **233**, 240–250.
- Nagano, M., Ishikawa, T., Fujiwara, M., Fukao, Y., Kawano, Y., Kawai-Yamada, M. and Shimamoto, K. (2016) Plasma membrane microdomains are essential for Rac1-RhoB/H-mediated immunity in rice. *Plant Cell* **28**, 1966–1983.
- Ndimba, B.K., Chivasa, S., Hamilton, J.M., Simon, W.J. and Slabas, A.R. (2003) Proteomic analysis of changes in the extracellular matrix of *Arabidopsis* cell suspension cultures induced by fungal elicitors. *Proteomics* **3**, 1047–1059.
- Neill, S., Barros, R., Bright, J., Desikan, R., Hancock, J., Harrison, J., Morris, P., Ribeiro, D. and Wilson, I. (2008) Nitric oxide, stomatal closure, and abiotic stress. *J. Exp. Bot.* **59**, 165–176.
- Okada, M., Matsumura, M., Ito, Y. and Shibuya, N. (2002) High-affinity binding proteins for N-acetylchitooligosaccharide elicitor in the plasma membranes from wheat, barley and carrot cells: conserved presence and correlation with the responsiveness to the elicitor. *Plant Cell Physiol.* **43**, 505–512.
- Paull, R.E., Chen, N.J., Ming, R., Wai, C.M., Shirley, N., Schwerdt, J. and Bulone, V. (2016) Carbon flux and carbohydrate gene families in pineapple. *Trop. Plant Biol.* **9**, 200–213.
- Peng, C.H. (2000) From static biogeographical model to dynamic global vegetation model: a global perspective on modelling vegetation dynamics. *Ecol. Modell.* **135**, 33–54.
- Rahman, M.H., Hjeljord, L.G., Aam, B.B., Sørli, M. and Tronsmo, A. (2015) Antifungal effect of chito-oligosaccharides with different degrees of polymerization. *Eur. J. Plant Pathol.* **141**, 147–158.
- Reese, T.A., Liang, H.E., Tager, A.M., Luster, A.D., Van Rooijen, N., Voehringer, D. and Locksley, R.M. (2007) Chitin induces accumulation in tissue of innate immune cells associated with allergy. *Nature* **447**, 92–96.
- Roby, D., Gabelle, A. and Toppan, A. (1987) Chitin oligosaccharides as elicitors of chitinase activity in melon plants. *Biochem. Biophys. Res. Commun.* **143**, 885–892.
- Sankaramakrishnan, N. and Sanghi, R. (2006) Preparation and characterization of a novel xanthated chitosan. *Carbohydr. Polym.* **66**, 160–167.
- Schauer, N., Zamir, D. and Fernie, A.R. (2005) Metabolic profiling of leaves and fruit of wild species tomato: a survey of the *Solanum lycopersicum* complex. *J. Exp. Bot.* **56**, 297–307.
- Shannon, P., Markiel, A., Ozier, O., Baliga, N.S., Wang, J.T., Ramage, D., Amin, N., Schwikowski, B. and Ideker, T. (2003) Cytoscape: a software environment for integrated models of biomolecular interaction networks. *Genome Res.* **13**, 2498–2504.
- Shi, H.T., Li, R.J., Cai, W., Liu, W., Wang, C.L. and Lu, Y.T. (2012) Increasing nitric oxide content in *Arabidopsis thaliana* by expressing rat neuronal nitric oxide synthase resulted in enhanced stress tolerance. *Plant Cell Physiol.* **53**, 344–357.
- Shibuya, N. and Minami, E. (2001) Oligosaccharide signalling for defence responses in plant. *Physiol. Mol. Plant Pathol.* **59**, 223–233.
- Shibuya, N., Ebisu, N., Kamada, Y., Kaku, H., Cohn, J. and Ito, Y. (1996) Localization and binding characteristics of a high-affinity binding site for N-acetylchitooligosaccharide elicitor in the plasma membrane from suspension-cultured rice cells suggest a role as a receptor for the elicitor signal at the cell surface. *Plant Cell Physiol.* **37**, 894–898.
- Shinya, T., Yamaguchi, K., Desaki, Y. et al. (2014) Selective regulation of the chitin-induced defense response by the Arabidopsis receptor-like cytoplasmic kinase PBL27. *Plant J.* **79**, 56–66.
- Sluiter, A., Hames, B., Ruiz, R., Scarlata, C., Sluiter, J., Templeton, D. and Crocker, D. (2008) Determination of structural carbohydrates and lignin in biomass. Technical Report, NREL/TP-510-42618. *Lab. Anal. Proc.* **1617**, 1–6.
- Soliman, M.H. and El-Mohamedy, R.S.R. (2017) Induction of defense-related physiological and antioxidant enzyme response against powdery mildew disease in Okra (*Abelmoschus esculentus* L.) plant by using chitosan and potassium salts. *Mycobiology* **45**, 409–420.

- Stacey, G. and Shibuya, N.** (1997) Chitin recognition in rice and legumes. *Plant Soil* **194**, 161–169.
- Tanaka, K., Gilroy, S., Jones, A.M. and Stacey, G.** (2010a) Extracellular ATP signaling in plants. *Trends Cell Biol.* **20**, 601–608.
- Tanaka, S., Ichikawa, A., Yamada, K., Tsuji, G., Nishiuchi, T., Mori, M., Koga, H., Nishizawa, Y., O'Connell, R. and Kubo, Y.** (2010b) HvCEBiP, a gene homologous to rice chitin receptor CEBiP, contributes to basal resistance of barley to *Magnaporthe oryzae*. *BMC Plant Biol.* **10**, 288.
- Tanaka, K., Choi, J., Cao, Y. and Stacey, G.** (2014) Extracellular ATP acts as a damage-associated molecular pattern (DAMP) signal in plants. *Front. Plant Sci.* **5**, 446.
- Thaware, D.S., Gholve, V.M. and Ghante, P.H.** (2016) Screening of chickpea varieties, cultivars and genotypes against *Fusarium oxysporum* f. sp. *Cicero*. *Int. J. Curr. Microbiol. App. Sci.* **5**, 896–904.
- Tonón, C., Terrile, M.C., Iglesias, M.J., Lamattina, L. and Casalongué, C.** (2010) Extracellular ATP, nitric oxide and superoxide act coordinately to regulate hypocotyl growth in etiolated *Arabidopsis* seedlings. *J. Plant Physiol.* **167**, 540–546.
- Truchet, G., Roche, P., Lerouge, P., Vasse, J., Camut, S., de Billy, F., Prome, J.C. and Dénarié, J.** (1991) Sulphated lipo-oligosaccharide signals of *Rhizobium meliloti* elicit root nodule organogenesis in alfalfa. *Nature* **351**, 670–673.
- Voxeur, A. and Fry, S.C.** (2014) Glycosylinositol phosphorylceramides from *Rosa* cell cultures are boron-bridged in the plasma membrane and form complexes with rhamnogalacturonan II. *Plant J.* **79**, 139–49.
- Walker-Simmons, M. and Ryan, C.A.** (1984) Proteinase inhibitor synthesis in tomato leaves. *Plant Physiol.* **76**, 787–790.
- Wan, J., Zhang, S. and Stacey, G.** (2004) Activation of a mitogen-activated protein kinase pathway in *Arabidopsis* by chitin. *Mol. Plant Pathol.* **5**, 125–135.
- Wu, S.J., Liu, Y.S. and Wu, J.Y.** (2008) The signaling role of extracellular ATP and its dependence on Ca²⁺ flux in elicitation of *Salvia miltiorrhiza* hairy root cultures. *Plant Cell Physiol.* **49**, 617–624.
- Xing, K., Li, T.J., Liu, Y.F. et al.** (2018) Antifungal and eliciting properties of chitosan against *Ceratocystis fimbriata* in sweet potato. *Food Chem.* **268**, 188–195.
- Yin, H., Zhao, X. and Du, Y.** (2010) Oligochitosan: a plant diseases vaccine-A review. *Carbohydr. Polym.* **82**, 1–8.
- Yin, H., Li, Y., Zhang, H.Y., Wang, W.X., Lu, H., Grevsen, K., Zhao, X. and Du, Y.** (2013) Chitosan oligosaccharides-triggered innate immunity contributes to oilseed rape resistance against *Sclerotinia Sclerotiorum*. *Int. J. Plant Sci.* **174**, 722–732.
- Yin, H., Du, Y. and Dong, Z.** (2016) Chitin oligosaccharide and chitosan oligosaccharide: two similar but different plant elicitors. *Front Plant Sci.* **7**, 522.
- Yoshioka, H., Mase, K., Yoshioka, M., Kobayashi, M. and Asai, S.** (2011) Regulatory mechanisms of nitric oxide and reactive oxygen species generation and their role in plant immunity. *Nitric Oxide* **25**, 216–221.
- Zeng, L., Velásquez, A.C., Munkvold, K.R., Zhang, J. and Martin, G.B.** (2012) A tomato LysM receptor-like kinase promotes immunity and its kinase activity is inhibited by AvrPtoB. *Plant J.* **69**, 92–103.
- Zhang, X., Li, K., Xing, R., Liu, S., Chen, X., Yang, H. and Li, P.** (2018) miRNA and mRNA expression profiles reveal insight into chitosan-mediated regulation of plant growth. *J. Agric. Food Chem.* **66**, 3810–3822.